The DOI for this manuscript is doi: 10.1175/JHM-D-12-0137.1

# Surface and atmospheric controls on the onset of moist convection over land

Pierre Gentine[1]
Department of Earth and Environmental Engineering
Columbia University
New York, NY, USA

Albert A.M. Holtslag
Meteorology and Air Quality Section
Wageningen University
Wageningen, the Netherlands

Fabio D'Andrea
Ecole Normale Supérieure, Ulm
Paris, France

Michael Ek
National Centers for Environmental Prediction
Suitland, MD, USA



[1] *Corresponding author address*: Pierre Gentine, Columbia University, 500W 120th Street, New York, NY 10027 USA
E-mail: pg2328@columbia.edu

## Abstract

The onset of moist convection over land is investigated using a conceptual approach with a slab boundary layer model. We here determine the essential factors for the onset of boundary layer clouds over land, and study their relative importance. They are: 1) the ratio of the temperature to the moisture lapse rates of the free troposphere, i.e. the inversion Bowen ratio, 2) the mean-daily surface temperature, 3) the relative humidity of the free troposphere and 4) the surface evaporative fraction. A clear transition is observed between two regimes of moistening of the boundary layer as assessed by the relative humidity at the boundary layer top. In the first so-called wet soil advantage regime, the moistening results from the increase of the mixed-layer specific humidity, which linearly depends on the surface evaporative fraction and inversion Bowen ratio through a dynamic boundary layer factor. In the second so-called dry soil advantage regime, the relative humidity tendency at the boundary layer top is controlled by the thermodynamics and changes in the moist adiabatic induced by the decreased temperature at the boundary layer top and consequent reduction in saturation water vapor pressure. This regime pertains for very deep boundary layers under weakly stratified free troposphere over hot surface conditions. In the context of the conceptual model, a rise in free-tropospheric temperature (global warming) increases the occurrence of deep convection and reduces the cloud cover over moist surfaces. This study provides new intuition and predictive capacity on the mechanism controlling the occurrence of moist convection over land.

# 1. Introduction

The land surface and the overlying atmosphere interact through a complex loop of feedback processes, which couple the energy and water cycles. The coupling between the land surface and the atmosphere is mediated by the state of the surface, which modifies the partitioning of the Surface Energy Budget (SEB) (Charney et al. 1975; Charney 1975; Delworth and Manabe 1989; 1993; Koster and Suarez 1994; Milly and Dunne 1994; Robock et al. 1995) and surface water budget (Rodríguez-Iturbe et al. 1999a; Rodríguez-Iturbe 2000; Laio et al. 2001; Porporato et al. 2004; Katul et al. 2007; Rigby and Porporato 2006) over timescales ranging from seconds/minutes to seasonal/interannual (Xue and Shukla 1993; Delire et al. 2004; Notaro 2008; Katul et al. 2007) and on spatial scales ranging from millimeters to hundreds of kilometers (Li and Avissar 1994; Rodríguez-Iturbe et al. 1995, 1999, 2006; Avissar 1995; Plaza and Rogel 2000; Wheater et al. 2000; Western et al. 2002, 2004; Ronda et al. 2002; Skoien et al. 2003; Isham et al. 2005).

The variations in land-surface properties modify the water and energy flux partitioning at the land surface, which affect the state of the overlying atmosphere (turbulence, heat, moisture, stability, clouds, precipitation, dynamics) (Gentine et al. 2007; 2010; 2011b; Findell et al. 2011; Gentine et al. 2011a) and the near-surface turbulence, temperature and moisture profiles (Businger et al. 1971). In turn, the change in the atmospheric state, mostly within the Planetary Boundary Layer (PBL), affects the surface heat and moisture transport on possibly different spatial and temporal scales (Boers et al. 1995; Raupach and Finnigan 1995; 1995; Wulfmeyer 1999; Petenko and

Bezverkhnii 1999; Sorbjan 2008; Paradisi et al. 2012; Katul et al. 1994a,b, 1999; Katul and Parlange 1995).

Boundary-layer clouds exert an important radiative feedback onto the land surface through the decreased shortwave incoming solar radiation and increased longwave radiation (Mahrt 1991; Ek and Mahrt 1994) but also impact the large-scale dynamics (Bony and Emanuel 2005). The occurrence of boundary-layer clouds is in turn related to the state of the land surface and especially on the surface turbulent heat flux partitioning, and consequently on the soil moisture state (Rabin et al. 1990; Ek and Holtslag 2004).

Shallow cumuli precondition the atmosphere for deep convection through moistening and heating of the free troposphere (Rio et al. 2009; Wu et al. 2009). Moist convection thus plays a prominent role in the radiative and hydrologic land-atmosphere coupling. The comprehension of the mechanisms triggering the onset of continental moist convection has nevertheless resisted a full theoretical treatment to date. This difficulty in the comprehension owes to the complicated and nonlinear boundary layer response to surface heat flux partitioning, which impacts both the rate of growth of the boundary layer as well as the condensation level in a non-trivial manner (van Heerwarden et al. 2008, 2009).

Using a tendency equation of the relative humidity at the boundary layer top, Ek and Mahrt (1994) followed by Ek and Holtslag (2004) demonstrated the role of direct surface moistening and boundary layer entrainment on the likelihood of cumulus onset. Huang and Margulis (2011) used this tendency equation to determine the evolution of the relative humidity at the top of the boundary layer in a series of large-eddy simulation experiments. Ek and Holtslag (2004) and Huang and Margulis (2011) highlighted the role

of free-tropospheric stability on the occurrence of moist convection either over a dry or wet soil. Westra et al. (2012) used field observations to illustrate, for the first time, to illustrate the increase in relative humidity at the boundary layer top over a drier soil, which we will refer to as a "dry soil advantage". Other studies (Chagnon et al 2005, Wang et al 2009) hinted towards the existence of the dry advantage regime by satellite observation of shallow cloud occurrence over forested and deforested areas in the Amazon. A dry advantage regime was also documented through the sensitivity integration of a regional model under heatwave conditions in Europe (Stefanon et al 2012).

The relative humidity tendency equation used in Ek and Holtslag (2004), is composed of an instantaneous surface evaporative term (evaporative fraction) and a "non-evaporative" boundary layer entrainment term. Although the evaporative fraction is often nearly constant during daytime (Gentine et al. 2007, 2011a), the boundary layer-entrainment term is typically varying throughout the day. Since the non-evaporative term is not preserved throughout the course of the day, instantaneous observation of the boundary layer state using radio-sounding, along with the tendency equation, are unable to clearly discriminate between the dry and wet soil advantage. On top of that, the boundary layer dynamics is itself dependent on the evaporative fraction, so that the non-evaporative term is not really disentangled from the evaporative one. In order to resolve this issue, the boundary layer dynamics needs to be taken into account in the relative humidity tendency equation.

The main objective of this work is to explicitly delineate the conditions leading to either dry or wet soil advantage in the triggering of moist convection based on surface or

atmospheric observations that would be available anytime during the course of a day (free tropospheric sounding, evaporative fraction). By moist convection we here refer to any type of convective boundary layer cloud formation, as well as to the triggering of deep convection. We will show that the use of conserved variables and the boundary layer dynamics permit to objectively conclude whether moist convection will preferentially occur over a dry or moist surface and we will highlight the role of the free-tropospheric moisture and temperature, which were missing in earlier results. This study will also show that the response is highly non-linear in terms of surface evaporative fraction and free-tropospheric conditions.

The first part of the manuscript revisits the work of Ek and Mahrt (1994) and Ek and Holtslag (2004) and provides a tractable diurnal solution of the relative humidity tendency at the boundary layer top in terms of conserved variables. The resolution includes the dynamics of the boundary layer using the analytical formulation of the boundary layer evolution of Porporato (2009). The second part of the paper describes the diurnal cycle of relative humidity at the boundary layer top and the timing of boundary-layer cloud onset over land as a function of surface and atmospheric conditions. The threshold between wet soil and dry soil advantages is explained in terms of dynamic and thermodynamic factors. In the last section, the surface and atmospheric conditions favoring the occurrence of stratocumulus, fair-weather cumuli, shallow and deep cumulus are discussed providing practical applications and new insights on the mechanisms at play in the formation of boundary-layer clouds and convection over land.

# 2. Datasets

*a. African Monsoon Multidisciplinary Analysis (AMMA)*

In order to investigate the increase of relative humidity over either dry or wet surfaces we use data from the African Monsoon Multidisciplinary Analysis (AMMA) field campaign. We here briefly describe the dataset used in this study. The reader is referred to Westra et al. (2012) for more details on the dataset. The observations used were gathered on June 20, 22, 24 and 25, 2006 at the AMMA site of Niamey international Airport (13.477°N, 2.175°E, 225m above sea level). FIG. 1 depicts the early–morning radiosoundings of the four days. The soundings were launched at 0733 UTC on June 20, 0835UTC on June 22, 0834 UTC on June 24 and 0833 UTC on June 25.

June 20, 2006 was a clear-sky and hot day with temperatures of 27.3°C in the early morning (0600 UTC) and 38.2°C in the afternoon (1500 UTC) as observed with an eddy covariance system of the Atmospheric Radiation Measurement (ARM) Program mobile facility setup just outside Niamey airport. The relative humidity at the surface was similar to other days. It should be emphasized that the sounding of June 20 on FIG. 1 was taken an hour before the other soundings so that the surface temperature appears lower and the relative humidity higher than in other soundings. After the rise of the boundary layer the surface humidity conditions were similar in the different days. The surface was dry on June 20 with a surface evaporative fraction of 0.1. The atmospheric mixed layer reached 1600m at 1828UTC. The early-morning lapse rate of potential temperature

between 1000 and 3000m was 3K/km as seen in FIG. 1. The inversion Bowen ratio, $B_{\text{inv}} = C_p \frac{\partial \theta}{\partial z} \Big/ \left| L_v \frac{\partial q}{\partial z} \right|$ (Betts 1992), was 0.96 within this layer.

A mesoscale convective system occurred the night of June 21 bringing 5mm of rain. As a result, on June 22 the evaporative fraction was higher than on other days, reaching 0.3. The early-morning lapse rate of potential temperature between 1000 and 3000m was 2.75K/km as seen in FIG. 1. The inversion Bowen ratio within this layer was 1.47. The mixed layer reached 1800m at 1740UTC. The temperature was higher that day reaching 40°C at 1500UTC and the day was clear. On June 24 and June 25 the surface was dry again and the evaporative fraction reached 0.1. On June 24 the air temperature reached 40°C. The early-morning lapse rate of potential temperature between 1000 and 3000m was 2.95K/km, similar to previous days. June 25 was extremely hot and the air temperature reached 44°C at 1400UTC. On June 24 the mixed layer reached 1700m at 1731UTC and a layer of shallow cumulus clouds developed in the morning. That day the early morning sounding was moister than on June 20 and 22. The inversion Bowen ratio between 1000 and 3000m was much higher than in previous days and reached 1.8. On June 25 the mixed layer was much higher than on other days and reached 2600m at 1745UTC. The high boundary layer was induced by the weak free-tropospheric stability (2.15K/km), as seen in FIG. 1. The inversion Bowen ratio was low (0.75) and the day was clear.

*b. Cabauw*

We use a second contrasting dataset located at Cabauw in the Netherlands to illustrate the onset of boundary-layer clouds in more humid and colder conditions. The

data were observed on May 31, 1978. The reader is referred to EH04 for details on the observations. Four radiosondes were launched from the Cabauw site during the morning of the study day providing temperature and moisture profiles above the tower level. Additionally the dataset is supplemented with information from radiosondes launched at De Bilt (about 25 km to the northeast) several times during the day, providing additional measurements of wind, temperature, and moisture. Sensible and latent heat fluxes determined from profile and Bowen ratio methods. The 20m air temperature reached 26°C at 1600UTC and the specific humidity was fairly constant between 7 to 8g/kg during the course of the day. A fair-weather cumulus cloud layer developed at 1500UTC. The surface was humid and the evaporative fraction was fairly constant during daylight hours at 0.8. The free-tropospheric potential temperature lapse rate was 3.7 K/km and the specific humidity lapse rate was -1.6 g/kg/km. The inversion Bowen ratio was 0.93.

# 3. Relative humidity at mixed-layer top

## *a. Background*

In order to investigate the occurrence of boundary-layer clouds over land we start with the relative humidity tendency equation at the boundary layer top as formulated by Ek and Holtslag (2004) (referred to as EH04 hereafter), which is based on the earlier tendency equation of Ek and Mahrt (1994). The relative humidity tendency is based on a slab zero-th-order model of the boundary layer, under negligible advection and vertical motion, with a potential temperature and specific humidity jump $\Delta q$ at the mixed layer top $h$ (Lilly 1968; Betts 1973; Deardorff 1979). The model is depicted in FIG. 2. A list of

all symbols and variables is available in Table 1. The tendency of the relative humidity at the boundary layer top, $RH(h)$, is:

$$\frac{\mathrm{d}RH(h)}{\mathrm{d}t} = \frac{R_n - G}{\rho L_v h q_s}\left[EF + \mathrm{ne}(1-EF)\right] \quad (1)$$

where ne represents the non-evaporative terms:

$$\mathrm{ne} = \frac{L_v}{C_p}(1+\alpha)\left[\frac{\Delta q}{h\gamma_\theta} + RH(h)\left(\frac{c_2}{\gamma_\theta} - c_1\right)\right]. \quad (2)$$

The parameters $c_1$ and $c_2$ are:

$$c_1 = \frac{L_v}{R_v}\frac{q_s}{T^2}\left(\frac{p(h)}{p_0}\right)^{R_d/C_p} \quad (3)$$

and

$$c_2 = \left(\frac{L_v}{R_v}\frac{q_s}{T^2} - \frac{C_p}{R_d}\frac{q_s}{T}\right)\frac{g}{C_p}. \quad (4)$$

Equation (1) above has provided important insights on the formation of boundary-layer clouds over land. However, its main drawback is that the non-evaporative term, ne, depends on both surface and atmospheric conditions and on the boundary layer dynamics. As such the non-evaporative term can vary and even change sign during the course of the day. As a consequence the non-evaporative term can either moisten or dry up the boundary layer, enhancing or reducing the likelihood of boundary-layer cloud onset. This has led to inconclusive diagnostics of the boundary layer moistening, as highlighted by Westra et al. (2012).

Our main goal here is to define the occurrence of cumulus onset and increase of $RH(h)$ as a function of conserved variables that could be observed anytime throughout the day using early-morning radio-sounding, for instance. To do so we will relate the

boundary layer dynamics to the surface evaporative fraction using the conceptual model of the convective boundary layer of Porporato (2009) (referred to as P09 hereafter).

*a. Impact of boundary-layer dynamics*

Neglecting the early-morning transition between the stable and unstable boundary layer and assuming a linear free-tropospheric profile of potential temperature: $\theta_{\text{free troposphere}}(z) = \theta_{f0} + \gamma_\theta z$, the mixed-layer potential temperature ($\overline{\theta}$) is linearly related to the mixed layer height (*h*) as (P09):

$$\overline{\theta} = \theta_{f0} + \gamma_\theta ' h \tag{5}$$

with

$$\gamma_\theta ' = \frac{1+\alpha}{1+2\alpha}\gamma_\theta , \tag{6}$$

and $\theta_{f0}$ is the ground intercept of the linear atmospheric profile (refer to FIG. 2). The entrainment efficiency $\alpha$ is the absolute ratio of the top of the boundary layer buoyancy flux to the surface value. The free-troposphere potential temperature lapse rate is assumed constant during the day. Since the entrainment coefficient and free-tropospheric potential temperature lapse rate are positive, $\gamma_\theta '$ is always positive. Boundary layer growth therefore always induces a warming of the boundary layer.

Evaporative fraction *EF*, the ratio of latent heat flux to available energy, $A = R_n - G = H + \lambda E$, at the surface is often relatively constant for daytime fair-sky conditions (Crago 1996; Crago and Brutsaert 1996; Lhomme and Elguero 1999, Gentine et al. 2007; 2011a). In the case of preserved evaporative fraction (or Bowen ratio *B* = (1-*EF*)/EF) and under a linearly stratified specific humidity free-tropospheric profile,

244 $q_{\text{free troposphere}}(z) = q_{f_0} + \gamma_q z$, the mixed-layer specific humidity is linearly related to the
245 mixed-layer height:

246 $$\overline{q} = q_{f0} + \gamma_q ' h \tag{7}$$

247 with

248 $$\gamma_q ' = \frac{1}{2}\left( \gamma_\theta \frac{C_p\, EF}{L_v(1+2\alpha)(1-EF)} + \gamma_q \right). \tag{8}$$

249

## 250 4. Tendency equation in terms of conserved variables

251 *a. Derivation*

252 In order to highlight the role of conserved variables on the relative humidity
253 tendency, we further simplify the issue by assuming a typical parabolic shape for the
254 available energy at the surface, again as in P09:

255 $$A(t) = A_0 \left[ 1 - \left( \frac{t}{t_0} - 1 \right)^2 \right], \tag{9}$$

256 where $A_0$ is the maximum diurnal available energy at the surface, $t$=0 corresponds to
257 sunrise, t=2t$_0$ to sunset, and $t_0$ is solar noon. This simple parabolic function leads to a
258 clean analytical solution for the boundary-layer height:

259 $$h(t) = \frac{2}{3}\left[ \frac{(1+2\alpha)(1-EF)A_0(3t_0 - t)t^2}{\rho C_p \gamma_\theta t_0^2} \right]^{1/2}. \tag{10}$$

260 This expression can be used to simplify the EH04 relative humidity tendency equation at
261 the mixed-layer top (1) and to introduce conserved variables. First, the specific humidity
262 jump at the boundary layer top can be written as a function of the mixed-layer height:

$$\Delta q = (\gamma_q{}' - \gamma_q)h\,, \tag{11}$$

which substituting (8) and (10) into (11), can be written as:

$$\Delta q = \frac{1}{2}\left(\gamma_\theta \frac{C_p}{L_v}\frac{1}{1+2\alpha}\frac{EF}{1-EF} - \gamma_q\right)h\,. \tag{12}$$

Next, substituting the above equation into (1) yields:

$$\frac{\mathrm{d}RH(h)}{\mathrm{d}t} = \frac{A(t)}{\rho L_v h\, q_s}\left[\begin{array}{l} EF\left(\dfrac{3+5\alpha}{2(1+2\alpha)}\right) \\ +\dfrac{1}{B_{ent}}\dfrac{1+\alpha}{2}(1-EF) \\ +(1+\alpha)(1-EF)RH(h)\dfrac{L_v}{C_p}\left(\dfrac{c_2}{\gamma_\theta}-c_1\right)\end{array}\right]. \tag{13}$$

Note that the first term before the brackets is the reverse of a time scale, which is increasing during the day. The terms c1 and c2 are described as a function of conserved variables in appendix B.

Equation (13) demonstrates that the diurnal course of relative humidity at the boundary layer top is monotonic throughout the course of the day. The ratio $A(t)/h(t)$ does not change sign during the course of the day, and neither do the factors in the brackets of the RHS. If the PBL experiences moistening (drying), in terms of relative humidity, this moistening (drying) lasts until sunset. Once boundary-layer clouds appear, the PBL humidity is mitigated by the cloud-base convective mass flux (Betts 1973; Arakawa 1974).

Equation (13) can be further expanded and described in terms of the time of day $t$ and of the conserved variables yielding:

$$\frac{\mathrm{d}RH(h)}{\mathrm{d}t} = \frac{\sqrt{C_p}}{\sqrt{\rho}\, L_v\, q_s} \frac{3}{2} \frac{\sqrt{A_0}\sqrt{\gamma_\theta}}{\sqrt{(1-EF)(1+2\alpha)}} \frac{2t_0 - t}{t_0\sqrt{(3t_0 - t)}} \left[ \begin{array}{l} EF\left(\dfrac{3+5\alpha}{2(1+2\alpha)}\right) \\ +\dfrac{1}{B_{ent}}\dfrac{1+\alpha}{2}(1-EF) \\ +(1+\alpha)(1-EF)RH(h)\dfrac{L_v}{C_p}\left(\dfrac{c_2}{\gamma_\theta} - c_1\right) \end{array} \right] . \quad (14)$$

The relative humidity tendency at the boundary layer top can now be described as a function of conserved variables at the surface (*EF* and $A_0$) and in the free troposphere ($\theta_{f0}$, $\gamma_\theta$, $q_{f0}$, $\gamma_q$) and as a function of time *t*. Equation (14) is a major improvement over previous formulations of the relative humidity tendency since it accounts for the boundary layer dynamics, as imposed by the surface evaporation and inversion Bowen ratio, using conserved variables only. This new equation gives an integrated view of the diurnal dynamics of the boundary layer on the relative humidity tendency, which was missing in previous studies.

*b. Timing of cloud onset*

Equation (14) can be integrated analytically (not shown) in time, giving the evolution of *RH*(*h*) throughout the day. The time for which RH is equal to 100% is the time of cloud occurrence and can be found by inverting the integral of (14). FIG. 3 depicts the time of cloud occurrence as a function of EF and the atmospheric stability ($\gamma_\theta$), free-tropospheric relative humidity $\overline{RH}$ and free-tropospheric surface potential temperature $\theta_{f0}$.

For visualization purposes, we only use a single variable to describe the humidity in the free troposphere, $\overline{RH}$, which represents the free-tropospheric relative humidity extrapolated down to the surface. The specific humidity lapse rate, $\gamma_q$, also needs to be computed. As in Brown et al. (2002) we specify a minimum specific humidity reference

value of 3 g/kg in the free troposphere at 3000m. This reference level is located above the typical diurnal peak of the dry boundary layer. $\gamma_q$ is then computed as the linear regression between the specific humidity at the surface and at the reference level. The results presented here are relatively insensitive to the reference specific humidity value chosen.

Everything else held constant, the time of cloud occurrence increases with increased stability, since the latter reduces the boundary layer growth and the possibility to reach the LCL. The entrained warm air also increases the saturation specific humidity through the Clausius-Clapeyron relationship. As a consequence the relative humidity is decreased.

The time of cloud occurrence exhibits two opposite behaviors in response to EF. Under strong free-tropospheric stability ($\gamma_\theta$ > 4-5K/km), the time of cloud occurrence is reduced under rising EF. The moisture provided by the surface latent heat flux compensates for the dry air entrainment resulting in earlier higher relative humidity. Oppositely, under weak free-tropospheric stability ($\gamma_\theta$ < 4-5K/km) the time of moist convection onset rises with increased EF. Reduced free-tropospheric stability facilitates the growth of the boundary layer and the entrainment of free-tropospheric air. This dry and warm entrained air reduces the relative humidity through the reduction of the mixed-layer specific humidity (by moisture conservation) and through the rise of the saturation specific humidity (by heat conservation in the mixed layer and through the Clausius-Clapeyron relationship). At high EF values (above 0.6 to 0.8 depending on the surface free-tropospheric relative humidity and temperature) the time of cloud occurrence rises

sharply in response to increasing EF and $\gamma_\theta$. In those conditions there is significant control of the surface on the exact timing of cloud occurrence.

A moistened free troposphere (higher $\overline{RH}$ ) favors the occurrence of clouds in any conditions and can modify the sign of the sensitivity of the timing of cloud onset to EF. Under wetter free tropospheric conditions, high EF values favor the occurrence of boundary layer clouds under strong stability, whereas the sensitivity is negative under a dry free troposphere. The moisture profile in the free troposphere is thus a key control of the sensitivity of cloud onset and the relative humidity tendency to surface evaporative fraction.

A warmer troposphere, as assessed by $\theta_{f0}$, leads to a reduction of boundary layer cloud onset. The reduction in low-cloud cover is consistent with recent results of global warming scenarios in climate models (Brient and Bony 2012). Our results suggest that the reduction will be especially pronounced over moist surfaces (EF>0.5) and under dry free tropospheric conditions. It could thus be expected that the early dry season will show a reduction of cloud cover over land under global warming. Of course our approach is only one-dimensional and does not include any horizontal circulations, which could alter the results presented here (Betts 2004).

FIG. 4 shows the Lifting Condensation Level (LCL) at the time of cloud occurrence. A strong sensitivity to the surface is observed in most cases beside at low EF values (left part of the plots). As EF increases the PBL depth is reduced and therefore the LCL decreases as well at the time of occurrence. Significant sensitivity to surface conditions is observed at high EF values and under stronger free-tropospheric stability.

*c. Moist and dry soil advantage regimes*

One of the most important results of EH04 and Westra (2012) is the somewhat counterintuitive realization that in some cases drier soils may favor the occurrence of boundary-layer clouds. These studies provided an important step forward in the understanding of the mechanisms controlling the likelihood of moist convection onset as a function of the surface and free-tropospheric state. They introduced the idea of different regimes of sensitivity to the soil wetness. Here, we will call them the "wet soil advantage" or "dry soil advantage" regimes. The exact limits between the two regimes remained unclear because the non-evaporative term of the tendency equation of EH04 varies throughout the course of the day and depends on the surface state through the boundary layer dynamic control. In order to describe the transition between the two regimes, we reinvestigate the sensitivity of the relative humidity at the mixed layer top using (14). The sign change of $\frac{dRH(h)}{dEF}$ defines the boundary between the two regimes as a function of conserved variables. The determination of the factors influencing the relative humidity at the mixed-layer top is described in the appendix. In summary, the PBL height and LCL depend on EF, on the free-tropospheric conditions and on the time of day. The relative humidity sensitivity at solar noon is used as a compact measure of the influence of the surface and free-tropospheric conditions. The relative humidity sensitivity exhibits weak dependence to the time of day. The main conserved variables contributing to the change of sensitivity are EF and the free-tropospheric conditions.

FIG. 5 depicts the separation between the two regimes, i.e. where the sensitivity vanishes: $\frac{dRH(h)}{dEF} = 0$. The region denoted with a plus (upper right part of the figure)

366 depicts a positive sensitivity to EF and therefore a wet soil advantage regime. The region
367 denoted with a minus depicts a dry soil advantage. We here loosely use the wet surface
368 terminology for high EF values and dry surface for low EF values even though we are
369 aware that other factors may impact the value of EF (entrainment, net radiation intensity,
370 etc). Those factors are discussed in detail in Lhomme and Elguero (1999), Raupach
371 (2000) and Gentine et al. (2007, 2011a).

372 Wetter surfaces (higher EF) exhibit higher relative humidity under strong free-
373 tropospheric stability ($\gamma_\theta$) and over very wet surface (high EF), consistent with the
374 observations of EF04 over Cabauw, the Netherlands (see below). EH04, Huang and
375 Margulis (2011) and Westra et al. (2012) have already emphasized the role of the free-
376 tropospheric stability on the relative humidity tendency.

377 FIG. 5 demonstrates that the reference surface EF plays an important role in the
378 control on $RH(h)$: calculating the sensitivity of the relative humidity $RH(h)$ to surface EF
379 yields opposite results between low and high reference EF values thus displaying an
380 important nonlinear response. The wet soil advantage region increases (in terms of
381 interval of EF) with decreasing free-tropospheric relative humidity, $\overline{RH}$, and with the
382 free troposphere temperature.

383 In summary the wetter soil advantage regime is more likely under dry and cold
384 free-tropospheric conditions and over wet surfaces (at large EF values). Conversely, drier
385 soil advantage is more likely under weak stability, moist and warm free troposphere and
386 over low-EF surfaces (lower left part of FIG. 5). The three important points to be
387 underlined are: 1) the reference EF value is important to determine the sign of the
388 sensitivity since the sensitivity is highly nonlinear, 2) the humidity and 3) reference

389 temperature of the free troposphere play crucial roles in the evolution of the relative
390 humidity at the top of the boundary layer.

391 For fixed free-tropospheric conditions and weak stability ($\gamma_\theta$<3.5-4K/km). The
392 change of sign of $\frac{dRH(h)}{dEF}$ while spanning the entire range of EF values indicates that
393 RH(EF) has a minimum for intermediate values of EF (around the root of $\frac{dRH(h)}{dEF}$).
394 Consequently, dry surfaces (e.g., urban) will likely exhibit higher mixed-layer top, higher
395 relative humidity and more likelihood of cloud occurrence than intermediate EF values.
396 At the same time, very moist surfaces (e.g. lakes) will also favor moist convection onset.
397 Under higher free-tropospheric stability ($\gamma_\theta$>4K/km), moist convection is always favored
398 over moister surfaces (with larger EF). These new results provide important physical
399 intuitions onto the likelihood of boundary-layer cloud onset over land under varying
400 environmental conditions.

401 Relative humidity increase over dry soil has recently been observed during the
402 African Monsoon Multidisciplinary Analyses (AMMA) measurement campaign in the
403 semiarid Sahel (Redelsperger et al. 2006). On June 20, 2006 relative humidity increased
404 at the boundary layer top over a dry soil (EF~0.1). The free troposphere was
405 characterized by relatively weak stratification ($\gamma_\theta$=3.4K/km), medium range relative
406 humidity ($q_{f0}$=14.36g/kg, $\overline{RH}$=56%) and was warm ($\theta_{f0}$=30°C). This day is represented
407 by a dot in FIG. 5 and falls in the dry soil advantage.

408 In contrast to the dry soil advantage, EF04 illustrated observations of a wet soil
409 advantage in Cabauw, the Netherlands over May 31, 1978. The evaporative fraction was
410 high (EF~0.8). The free-tropospheric conditions were reasonably warm ($\theta_{f0}$=17°C), with

low stratification ($\gamma_\theta$=4K/km). The environment was reasonably moist ($q_{f0}$=6.5g/kg, $\overline{RH}$ =61%). This day is also represented as a dot in FIG. 5 and falls within the moist surface advantage regime, confirming the potential of our simple model to characterize the occurrence of cloud and the tendency of relative humidity as a function of the state of the surface and of the atmospheric conditions.

Other recent observational studies showed that in some conditions, moist convection is favored over dry soils. This includes the observations of more frequent deep convection development in the Sahel (Taylor et al. 2011 and Taylor et al. 2012), and of higher shallow cumulus cover in the Amazon (Chagnon et al 2005, Wang et al 2009). In the Sahel, dryer and wetter patches of soil were compared. The patches had a spatial scale of 10 to 15 km, and hence share the same synoptic scale atmospheric forcing. Higher probability of triggering of convective storm is observed over dryer patches. This is assumed to be induced by mesoscale breezes created by differential heating on the ground that creates convergence on the dry side (Taylor et al. 2011, 2012). Our results suggest that there could be a concurrent mechanism of boundary layer moistening over drier soils induced by the one-dimensional boundary layer dynamics described above, given the dryness of the Sahel (low EF) and the weak stratification of the monsoon period. This mechanism could precondition or help the triggering of convection by the mesoscale features. Consistent with the above results, in a recent regional model study, Stefanon et al (2012) observed that a drying of the soil induces an increase of shallow cumulus activity. This result was found under the specific conditions of European heatwaves, with high temperatures, dry free troposphere and weak stratification over the whole continent. The mesoscale circulation, in this case, was found to reinforce

convection and precipitation over the mountains. On the other hand, the Amazon is characterized by high overall EF in the wet season. In case of very weak stratification (lower-right side of the diagram in FIG. 5) the system can bifurcate between dry and wet soil advantage regimes.

# 5. Dynamic versus thermodynamic moistening

*a. Direct mixed-layer specific humidity increase*

In contrast with the potential temperature, the boundary layer growth can either moisten or dry the boundary layer in terms of specific humidity (Mahrt 1991, Betts 1992). Since the mixed-layer specific humidity appears at the numerator of $RH(h)$ it is enlightening to evaluate the regimes of increase or decrease in boundary layer specific humidity.

The transition between the moistening and drying of the boundary layer (in terms of mixed-layer specific humidity) occurs when the RHS of (8) vanishes that is when:

$$L_v\gamma_q = -C_p\gamma_\theta \frac{1}{(1+2\alpha)} \frac{EF}{(1-EF)} = -C_p\gamma_\theta \frac{1}{(1+2\alpha)} \frac{1}{B_0}. \qquad (15)$$

This threshold value can be used to define a critical $EF$, $EF_c$, above which the boundary layer moistens (in terms of specific humidity). We introduce the inversion Bowen ratio of free-tropospheric air at the boundary layer top (Betts 1992; Betts and Ball 1994): $B_{\text{inv}} = -C_p\gamma_\theta / L_v\gamma_q > 0$, which is the ratio of the potential temperature free tropospheric lapse rate to the specific humidity free tropospheric lapse rate. $B_{\text{inv}}$ measures the ratio of the heating induced by the change in temperature and by the change in moisture, per unit height in the free troposphere. As such it is a critical factor controlling the moistening of

455 the boundary layer during its growth. Neglecting the density difference correction
456 induced by water vapor loading, the inversion Bowen ratio $B_{inv}$ is 0 for a dry adiabatic
457 profile, while it is 1 for a moist adiabatic profile corresponding to a constant equivalent
458 potential temperature (Betts 1992).

459 Inverting (15), the critical *EF* can be expressed in terms of $B_{inv}$ as:

460 $$EF_c = \frac{1+2\alpha}{1+2\alpha+B_{inv}} < 1 \qquad (16)$$

461 This critical value was found by P09 without the introduction of the inversion Bowen
462 ratio. Betts (1992) found such abrupt transition between the drying and moistening of the
463 boundary layer using a mixing-line analysis (Betts 1985) and the tendency of the specific
464 humidity in the mixed-layer. For any free-tropospheric stratification, the boundary-layer
465 specific humidity will increase when *EF* exceeds $EF_c$ and will decrease otherwise. This
466 moistening corresponds to the interplay between the surface moistening as assessed by
467 the evaporative fraction and competition through the boundary layer dynamics and the
468 dry and warm air entrainment at the boundary layer top. Since $B_{inv}$ increases in weakly
469 stable (smaller $\gamma_\theta$) and in moister (smaller $|\gamma_q|$) free troposphere conditions, $EF_c$ decreases
470 in those conditions and the mixed-layer specific humidity increases with similar *EF*
471 values. Since the specific humidity increases with *EF*, as seen in (8), drier soils will
472 always lead to a reduction of the specific humidity. As such the specific humidity
473 changes induce by the evaporative fraction and boundary layer dynamics entraining dry
474 air cannot explain the dry soil advantage.

475 In the AMMA dataset the early morning profile on June 24, 2006 exhibited the
476 highest inversion Bowen ratio (1.8), which corresponds to an $EF_c$ value of 0.44, still
477 much higher than the observed *EF* value (0.1). Consequently all of the AMMA days used

here induced a specific humidity drying over dryer surfaces. On the other hand, over the Cabauw site the inversion Bowen ratio was 0.96, which corresponds to a critical *EF* of 0.59, lower than the observed *EF* value (0.8). Moister surfaces in this case led to a direct increase of the boundary layer specific humidity through the reduction in boundary layer height.

1. Limiting $EF_c$ cases: Dependence on entrainment parameter $\alpha$

We here examine some limiting cases of the critical $EF_c$. We first consider the case of pure encroachment, when the entrainment $\alpha$ vanishes. In this case $EF_c$ reaches $1/(1+B_{inv})$. In other words, the critical surface Bowen ratio $B_0$ exactly compensates for the inversion Bowen ratio $B_{\mathrm{inv}}$. When the surface Bowen ratio is higher (that is $EF<EF_c$) the boundary layer dries up. The boundary layer growth induces the entry of dry free tropospheric air into the boundary layer, as an open system. The boundary layer moistens in the opposite case when $EF>EF_c$ since the surface moistening overcomes the entry of dry free-tropospheric air. When entrainment at the boundary layer top becomes very large, $\alpha \to \infty$, the critical *EF* value approaches unity. The entrainment dominates the surface moistening in all cases.

2. Limiting $EF_c$ cases: Dependence on inversion Bowen ratio

In the case of small inversion Bowen ratio, which corresponds to either a weak stability or dry free-tropospheric profile, $EF_c$ approaches unity and the boundary layer always dries up. The small inversion Bowen ratio induces rapid growth of the boundary layer and important drying associated with the large amount of entrained dry free-tropospheric air. The surface moistening cannot counterbalance the large quantity of entrained dry free-tropospheric air.

Large inversion Bowen ratio, in turn, implies a small $EF_c$. The strong stability induces a reduction of the dry air entrainment at the boundary layer top. A humid free-tropospheric profile prevents the reduction of the boundary layer specific humidity by entrainment. In all cases, insufficient free-tropospheric dry air is entrained within the boundary layer and cannot counteract the surface moistening.

It is important to stress that the boundary layer moistening in terms of specific humidity might be very different from the moistening in terms of relative humidity. The nonlinear response of the Clausius-Clapeyron relationship to temperature in the denominator of $RH(h)$ might indeed reduce the relative humidity even though the boundary layer experiences a specific humidity increase. In particular the linear mixing of dry air from the free troposphere and dry air from the mixed layer may be saturated because of the convexity of the Clausius-Clapeyron relationship. In addition, the relative humidity at the mixed-layer top depends on temperature, which decreases as the boundary layer deepens. Consequently, a deeper boundary layer might be more likely to generate boundary-layer clouds.

*b. Factors controlling the relative humidity tendency*

In order to further comprehend the mechanisms leading to the increase of relative humidity at the boundary layer top we get back to our new relative humidity tendency equation in terms of conserved variables (14). The first term in the brackets on the RHS of (14) is:

$$F_1 = EF\left(\frac{3+5\alpha}{2(1+2\alpha)}\right). \tag{17}$$

522 $F_1$ corresponds to the direct surface heat flux moistening (in terms of EF) on the PBL
523 relative humidity through the increase of the specific humidity. Increased EF induces a
524 direct moistening of the PBL in terms of relative humidity, as is expected.

525 The second term of the relative humidity tendency equation is:

526 $$\mathrm{F}_2 = \frac{1}{2}\frac{L_v}{C_p}\frac{\gamma_q}{\gamma_\theta}(1+\alpha)(1-EF) = -\frac{1}{2}\frac{(1+\alpha)(1-EF)}{B_{inv}} < 0\,. \qquad (18)$$

527 This term corresponds to the drying of the boundary layer induced by the entrainment of
528 dry free tropospheric air, as discussed in section 5a. The ratio of the two factors is
529 depicted in FIG. 6 as a function of the surface evaporative fraction and of the inversion
530 Bowen ratio. As expected, in regions of higher EF and higher $B_{\mathrm{inv}}$ the surface moistening
531 dominates the drying by entrainment $\mathrm{F}_2$. The Cabauw data point belongs to this region of
532 direct moistening increase. Regions of low EF and low $B_{\mathrm{inv}}$ on the other hand are mostly
533 impacted by the effect of entrained air since the boundary layer grows deeper. All of the
534 AMMA data points belong to this region of free-tropospheric influence, which induces a
535 drying of the boundary layer specific humidity.

536 The two factors can be combined to comprehend the limits of the drying or
537 moistening regimes of the boundary layer in terms of relative as opposed to specific
538 humidity described in section 5a. Both factors are related to the dynamic of the boundary
539 layer, either through direct surface moistening or through entrained free-tropospheric air.
540 This combined factor is thus called dynamic factor, as opposed to the thermodynamic
541 factor that is discussed below. The sum of (17) and (18) is:

542 $$F_{\mathrm{Dyn.}} = EF\left(\frac{3+5\alpha}{2(1+2\alpha)}\right) - \frac{1}{2}\frac{(1+\alpha)(1-EF)}{B_{inv}}\,. \qquad (19)$$

543 The dynamic control on the relative humidity tendency, $F_{\text{Dyn.}}$, increases linearly in *EF*
544 and changes sign at the threshold value:

545 $$EF_{\text{sign}} = \frac{(1+\alpha)(1+2\alpha)L_v\gamma_q}{(3+5\alpha)C_p\gamma_\theta + (1+\alpha)(1+2\alpha)L_v\gamma_q} = \frac{1}{1-B_{inv}\dfrac{3+5\alpha}{(1+\alpha)(1+2\alpha)}}. \qquad (20)$$

546 The dynamic control on the relative humidity tendency depends on the inversion
547 Bowen ratio $B_{\text{inv}}$ and on the entrainment efficiency $\alpha$. More efficient entrainment, such
548 as in the case of intense shear (Pino et al. 2006), displaces $EF_{\text{sign}}$ toward unity. A critical
549 value of $B_{\text{inv}}$ exists, $B_{inv}^{crit} = (1+\alpha)(1+2\alpha)/(3+5\alpha)$, below which $EF_{sign}$ is always
550 negative. $B_{inv}^{crit} \sim 0.42$ with a typical value of the entrainment efficiency $\alpha$=0.2. This
551 corresponds to a free troposphere in intermediate conditions between a dry adiabatic
552 lapse rate ($B_{\text{inv}}$ =0) and moist adiabatic ($B_{\text{inv}}$ =1). Below the critical $B_{\text{inv}}$ value, the
553 dynamic control increases the relative humidity over all types of surface. Above the
554 critical $B_{\text{inv}}$ value, dry soils (low EF) induce negative dynamic factor acting to reduce the
555 relative humidity at the boundary layer top though dynamic factors. In all cases though,
556 moister surfaces (higher EF) increase the dynamic control on relative humidity.

557 Since the dynamic control is linear and increasing with EF, the only reason for the
558 non-trivial behavior of the relative humidity tendency increasing over drier surfaces has
559 to do with the last term in the brackets of (14). We call this term the thermodynamic
560 factor:

561 $$F_{\text{Therm.}} = (1+\alpha)(1-EF)RH(h)\frac{L_v}{C_p}\left(\frac{c_2}{\gamma_\theta} - c_1\right). \qquad (21)$$

562 Let us first try to understand the physical meaning of this factor. The moist adiabatic
563 temperature lapse rate reads:

564 $$\Gamma_{\text{moist}} = \frac{g}{C_p}\frac{1+\frac{L_v q}{R_d T}}{1+\frac{L_v^2 q}{C_p R_d T^2}}. \quad (22)$$

565 A first-order Taylor approximation of it gives:
566

567 $$\Gamma_{\text{moist}} \approx \frac{g}{C_p}\left(1+\frac{L_v q}{R_d T}-\frac{L_v^2 q}{C_p R_d T^2}\right) \approx \Gamma_{\text{dry}}\left(1+\frac{L_v q}{R_d T}-\frac{L_v^2 q}{C_p R_d T^2}\right), \quad (23)$$

568 with $\Gamma_{dry} = g / C_p$ the dry adiabatic temperature lapse rate. The latter equation can be

569 rewritten into a more convenient form, which uses the relative humidity:

570 $$\Gamma_{\text{moist}} \approx \Gamma_{\text{dry}} + RH(h) q_s \frac{g}{C_p}\frac{1}{T}\frac{{L_v}^2}{C_p R_v}\left(\frac{R_v}{R_d}\frac{C_p}{L_v}-\frac{1}{T}\right). \quad (24)$$

571 The thermodynamic factor, (21), can be simplified using the above equation:

572 $$F_{\text{Therm.}} = (1+\alpha)(1-EF)\left(\frac{C_p(\Gamma_{\text{dry}}-\Gamma_{\text{moist}})}{L_v q_s / h}-\frac{L_v}{R_v}RH(h)h\frac{1}{T^2}\left(\frac{p(h)}{p_0}\right)^{R_d/C_p}\right). \quad (25)$$

573 The thermodynamic factor is thus composed of two terms. The first one,

574 $F^{1}_{\text{Therm.}} = (1+\alpha)(1-EF)\left(\frac{C_p(\Gamma_{\text{dry}}-\Gamma_{\text{moist}})}{L_v q_s / h}\right)$, represents the impact of the departure

575 between the dry and moist adiabatic on the relative humidity induced by the heating of

576 the boundary layer (1+$\alpha$)(1-*EF*). This factor is always positive and corresponds to an

577 increase of the relative humidity at the boundary layer top.

578 The second part of the thermodynamic factor, which is always negative,

579 corresponds to a relative humidity reduction induced by the air dilatation and cooling, as

580 the boundary layer deepens. This factor cannot explain the occurrence of moist

convection over dry soils since it acts to reduce the relative humidity at the boundary layer top.

The ratio between the two terms of the thermodynamic factor is plotted in FIG. 7. The ratio is plotted on a logarithmic scale and both factors are taken in absolute values. Interestingly, the departure between the dry and moist adiabatic is the dominant factor affecting the relative humidity tendency. The cooling of the actual temperature and dilatation at the boundary layer top is generally an order of magnitude smaller than the first term.

The departure between the dry and moist adiabatic is therefore the explanation for the occurrence of boundary-layer clouds over very dry regions in the presence of very deep boundary layers, such as over the Sahara (Cuesta et al. 2008). In this case the cloud cover is generally composed of fair weather cumuli and the cloud cover is highly positively correlated with the depth of the boundary layer since the temperature change at the boundary layer top strongly affects the moist adiabatic but not the dry adiabatic. This effect is also visible on FIG. 1. The relative humidity increases almost linearly with height in the mixed layer. This quasi-linear behavior is confirmed by later sounding in the afternoon (not shown here). It is then evident that if the boundary layer sufficiently deepens the relative humidity at the boundary layer top will reach a 100%, even though the amount of specific humidity can be very small like over the Sahara.

In order to differentiate regimes of dynamic or thermodynamic influence, the ratio of the two factors is plotted in FIG. 8. The ratio is plotted on a logarithmic scale and both factors are taken in absolute values. A positive value corresponds to a regime dominated by the dynamic factor. The dynamic factor is the main contributor of the relative

humidity tendency above a diagonal going from ($EF$=0, $\gamma_\theta$=4K/km) to ($EF$=1, $\gamma_\theta$=1K/km); that is in stable atmosphere with relatively wet surfaces. The thermodynamic factor is the main contributor below this diagonal; that is under weak stability and dry soil. The AMMA data points belong to the region of thermodynamic influences and therefore dryer surfaces can generate more clouds through the thermodynamic effect. On the other hand the Cabauw site belong to the region of dynamic influence and increased cloud cover occurs over moister surface through the direct surface moistening. Surprisingly, the diagonal does not evolve much with the increase of the free-tropospheric temperature and relative humidity. In fact, the EF and the free-tropospheric stability are the main contributors to the growth of the boundary layer, as established by equation (10), and it is the depth of the boundary layer that principally determines the influence of the thermodynamic factor through the difference between the dry and moist adiabatic. An important consequence is that the changes in surface temperature are small compared to the changes in temperature induced by an extended boundary layer growth under weak stability and low EF. Indeed a convective boundary layer has a nearly adiabatic profile, which corresponds to a temperature lapse rate of about 9.8K/km. Over deep boundary layers of a few kilometers the temperature reduction at the boundary layer top can be of the order a several tens of degrees, which can be much larger than surface temperature difference between hot and cold regions.

# 6. Forced versus active moist convection, stratocumulus to deep convection transition

Even though the relative humidity tendency at the boundary layer top provides important insights onto the development of boundary layer clouds, it cannot discriminate between stratocumulus, shallow or deep convection, or between forced and active clouds (Stull 1988). Forced clouds refer to thermal plumes that condensate but are negatively buoyant above their LCL. Those plumes have reached their LCL but have not overcome their convective inhibition (CIN) and have thus not reached the level of free convection (LFC). Forced cloud cover can be either stratocumulus or forced shallow convection clouds. Conversely, active clouds have overcome the CIN and have reached their LFC. Active convection can be shallow or deep and generates a cloud base mass flux used as the boundary condition for a most convective scheme (Betts 1973, Arakawa and Schubert 1974, Gentine et al. 2012a,b).

A useful indicator of the triggering of active convection vs. forced convection is the difference between the mixed-layer equivalent potential $\overline{\theta_e}$ and the saturation equivalent potential temperature just above the inversion $\theta_e^{sat}(h_+)$ (Emanuel 1994, D'Andrea et al. 2006). This difference is an indicator of the convective inhibition and conditional instability at the top of the boundary layer. Positive values indicate active convection and negative values refer to forced convection. The main difficulty of the saturation equivalent potential temperature is that it is nonlinearly dependent on the boundary layer height and therefore on the surface evaporative fraction and inversion Bowen ratio. The transition between the shallow and deep convection depends on the

645 strength of the convective inhibition and equivalent potential temperature lapse rate
646 above the boundary layer (Rio et al. 2009, Del Genio and Wu 2010, Hohenegger and
647 Bretherton 2011). A large positive $\overline{\theta_e}$ - $\theta_e^{sat}(h_+)$ is an indicator of deep convective
648 conditions, a smaller positive $\overline{\theta_e}$ - $\theta_e^{sat}(h_+)$ pertains to active shallow convection. A
649 small negative $\overline{\theta_e}$ - $\theta_e^{sat}(h_+)$ reflects the presence of fair-weather cumuli. Large negative
650 $\overline{\theta_e}$ - $\theta_e^{sat}(h_+)$ indicates the generation of stratocumuli.

651 The difference $\overline{\theta_e}$ - $\theta_e^{sat}(h_+)$ is plotted in FIG. 9. The bold line contour indicates the
652 crossover between positive and negative regions. Note the similarity of this figure with
653 FIG. 4. Dry free troposphere favors the occurrence of forced convection. In these
654 conditions active convection is impossible since it can only occur under a free-
655 tropospheric stability inferior to 1K/km, which is unachievable. A humid free troposphere
656 increases the likelihood of active convection with more intense conditional instability in
657 the presence of warm free-tropospheric conditions, as would be expected. Strong
658 subsidence, i.e. large stability, is generally associated with strong free-tropospheric
659 stability and with the presence of stratocumulus over the ocean (Stevens 2005). This is
660 also confirmed over land by our analysis.

661 The dependence of the conditional instability to the surface EF is again non
662 trivial. Under drier free-tropospheric conditions, a rise in EF increases the occurrence of
663 all clouds (less white contour), yet moister surfaces favor forced convection
664 (stratocumulus and forced shallow convection). Under humid ($\overline{RH} = 75\%$) free-
665 tropospheric conditions EF barely influences the occurrence of active convection, beside
666 over very wet surface (EF>0.7-0.8). As a consequence, very wet surface conditions

667 (EF>0.7) favor active convection under wet atmosphere (e.g. Amazon). Drier, warm free-
668 tropospheric conditions ( $\overline{RH} = 50\%$ and $\theta_{f0} = 20 - 30^{\circ}\mathrm{C}$ ) with weak stratification in turn
669 favor active convection over dry soil (e.g. Sahel - Taylor et al. 2012).

670 FIG. 9 can be useful to make hypotheses on the effect of global warming on the
671 occurrence of boundary–layer clouds, assuming other variables remain constant (e.g.
672 relative humidity, surface evaporative fraction, available energy at the surface and free-
673 tropospheric stability). FIG. 8 indicates a reduction of the occurrence of clouds over land
674 under global warming, especially over moist surfaces (high EF). The occurrence of deep
675 convection, as defined by the regions in red in FIG. 9, increases as recently observed over
676 land in climate model simulations (Wyant et al. 2012). Stratocumulus clouds also become
677 less frequent over land under increased free-tropospheric temperature. In our conceptual
678 model we do not account for the coupling with the large-scale circulations and the
679 advection to/from the ocean (Betts 1988, 1989, Lintner et al. 2012). The results have
680 therefore to be interpreted with caution.

# 681 7. Conclusions

682 The onset of moist convection is investigated using a mixed-layer model of the boundary
683 layer. To facilitate an analytic development, a constant evaporative fraction is assumed.
684 The sensitivity of the relative humidity at the boundary layer – defined by $\frac{\partial RH(h)}{\partial EF}$ - not
685 only depends on the free-tropospheric stability as demonstrated in previous studies but
686 also on the free-tropospheric moisture, on the temperature of the free troposphere and on
687 the reference EF used for the computation of the sensitivity. The relative humidity at the
688 top of the boundary layer exhibits two regimes, a dry soil advantage and a wet soil

advantage regime. The factors influencing the system to go into one or the other of these two regimes are either dynamic or thermodynamic.

The dynamic factor comes from the interplay between the direct effect of the surface on the specific humidity of the PBL, and the indirect effect via the boundary layer dynamics entraining drier and warmer free troposphere air. A dry surface, reduces the specific humidity, hence tends to reduce the relative humidity. At the same time, however, it will cause the boundary layer to grow, entraining free atmospheric air. This air, if cold and dry enough, can cause the relative humidity to increase because of the Clausius-Clapeyron relationship. The prevalence of the direct or of the indirect effect is mainly controlled by the inversion Bowen ratio and by the entrainment efficiency. The dynamic regime pertains to boundary layers that are not too deep and reflects the typical mechanisms of boundary layer moistening and low-level cloud generation. This process is similar to the generation of low-level cloud over the ocean through the increase of the specific humidity. The dynamic regime dominates over wet surfaces and strong free-tropospheric stability and is favored under moister and colder free troposphere. In this regime boundary-layer clouds and the relative humidity at the boundary layer top increase with a rise in surface evaporative fraction, that is over moister surfaces.

The second, thermodynamic factor, concerns deep boundary layer regimes such as observed over the Sahel and Sahara. In this regime the departure between the moist and dry adiabatic induces an opposite response to surface moistening and dryer soils favor the generation of boundary layer clouds since drier surfaces increase the boundary layer depth. Warmer and drier free troposphere reduces the likelihood of cloud occurrence with the thermodynamic control.

712 The timing of cloud occurrence is tightly related to the free-tropospheric
713 conditions (stability, temperature and humidity) and surface evaporative fraction. Moist
714 convection onset occurs earlier over moist surfaces (large EF values) in regimes of strong
715 free-tropospheric stability and cold environments. The opposite behavior is observed in
716 regimes of weak free-tropospheric stability and warm environments. Not surprisingly
717 boundary-layer cloud occurrence is disfavored under dry and cold free troposphere but
718 also under warm and moist free troposphere regimes.

719 Finally we discuss the occurrence of active convection (shallow or deep)
720 compared to forced convection (stratocumulus or fair-weather cumuli) as a function of
721 conserved variables. Very wet surface conditions (evaporative fraction larger than 0.7)
722 favor active convection under a wet atmosphere (e.g. Amazon). Drier, warm free-
723 tropospheric conditions with weak stratification in turn favor active convection over dry
724 soil. In the context of the one-dimensional model used in this paper, it is expected that
725 deep convection will increase over land under global warming, especially over dry
726 surfaces. On the other hand, the fraction of stratocumulus and shallow cumulus clouds is
727 expected to decrease over humid surfaces.

728

729

# APPENDIX A

## Derivation of critical EF

We here investigate the existence of one or multiple critical EFs such that the relative humidity tendency equation (13) vanishes. The main complication is due to the time dependence of the solution and the fact that the saturation specific humidity linearly depends on the PBL height and on its temperature. In order to simplify the resolution of those critical EF values, the relative humidity tendency equation (13) is rewritten in a more convenient form:

$$\frac{\mathrm{d}RH(h)}{\mathrm{d}t} = \frac{A(t)}{\rho L_v h\, q_s}\left[\begin{array}{l} EF\left(\dfrac{3+5\alpha}{2(1+2\alpha)}\right) \\ -\dfrac{L_v\gamma_q}{C_p\gamma_\theta}\dfrac{1+\alpha}{2}(1-EF) \\ +(1+\alpha)(1-EF)\dfrac{L_v q}{C_p T}\left(\left(\dfrac{L_v}{R_v}\dfrac{1}{T}-\dfrac{C_p}{R_d}\right)\dfrac{g}{C_p}\dfrac{1}{\gamma_\theta}-\dfrac{L_v}{R_v}\dfrac{1}{T}\left(\dfrac{p(h)}{p_0}\right)^{R_d/C_p}\right) \end{array}\right]. \quad \text{(A1)}$$

The mixed-layer specific humidity depends on EF, as seen in (7). The temperature T on top of the mixed layer also depends on the mixed-layer potential temperature, which itself depends on EF, and nonlinearly on the height of the mixed layer, which also depends on EF:

$$T = \theta\left[\frac{p(h)}{p_0}\right]^{R_d/C_p}. \quad \text{(A2)}$$

The dependence of the relative humidity tendency on EF is thus strongly nonlinear. An analytical solution cannot be obtained. Nonetheless we can numerically investigate

sensitivity of (A1) to EF and especially the values at which (A1) or the relative humidity vanish. Since the mixed-layer height is time dependent, the solution will most likely be time dependent. We choose to evaluate the EF values corresponding to a vanishing relative humidity tendency at solar noon $t_0$ for simplicity. Further tests showed that the conclusions only weakly depend on the time of day.

# APPENDIX B

## Dependence of $c_1$ and $c_2$ on conserved variables

We here derive the coefficients $c_1$ and $c_2$ as a function of conserved variables.

$$c_1 = \frac{L_v}{R_v}\frac{q_s}{T^2}\left(\frac{p(h)}{p_0}\right)^{R_d/C_p} \tag{25}$$

and

$$c_2 = \left(\frac{L_v}{R_v}\frac{q_s}{T^2} - \frac{C_p}{R_d}\frac{q_s}{T}\right)\frac{g}{C_p}\,. \tag{25}$$

The pressure at level $h$ can be related to the mixed-layer potential temperature using a hydrostatic assumption as:

$$p(h) = p_0 \exp\left(-\frac{gz}{R_d\overline{\theta}}\right). \tag{25}$$

The mixed-layer potential temperature is related to conserved variables using equations (5) and (10). The absolute temperature $T$ at the top of the mixed layer is simply related to the mixed-layer potential temperature by definition of the potential temperature:

765 $$T = T(h) = \bar{\theta}\left(\frac{p(h)}{p_{\text{ref}}}\right)^{R_d/C_p}. \quad (25)$$

766 The saturation specific humidity is simply related to the temperature and pressure on top
767 of the mixed layer using the Clausius-Clapeyron relationship and is therefore expressed
768 in terms of the mixed-layer potential temperature and to conserved variables again using
769 equations (5) and (10).

770

771 *Acknowledgments.*

772 This work has been carried out as part of grant *NSF*-AGS-1035986 of the National
773 Science Foundation. The authors wish to thank Alan K. Betts for his comments on the
774 manuscript as well as Françoise Guichard and Gert-Jan Steeneveld for providing the
775 AMMA data used in this analysis.

776

# References

Arakawa, A., 1974: Interaction of a cumulus cloud ensemble with the large-scale environment, Part I. *J Atmos Sci*, **31** (3), 674-710.

Avissar, R., 1995: Scaling of Land Atmosphere Interactions - an Atmospheric Modeling Perspective. *Hydrol Process*, **9**, 679–695.

Betts, A. K., 1973: Non-precipitating cumulus convection and its parameterization. *Q J Roy Meteor Soc*, **99**, 178–196.

Betts, A. K., 1985: Mixing-line analysis of clouds and cloudy boundray layers. *J Atmos Sci*, **42** (24), 2751–2763.

Betts, A. K., & Ridgway, W. (1988). Coupling of the Radiative, Convective, and Surface Fluxes over the Equatorial Pacific. *http://dx.doi.org/10.1175/1520-0469(1988)0452.0.CO;2*.

Betts, A. K., & Ridgway, W. 1989: Climatic Equilibrium of the Atmospheric Convective Boundary Layer over a Tropical Ocean, *J Atmos Sci,* **46**(17), 2621-2641.

Betts, A. K., 1992: FIFE atmospheric boundary layer budget methods. *J Geo Res-Atmos*, **97** (D17), 18523–18531.

Betts, A. K., and J. Ball, 1994: Budget Analysis of Fife-1987 Sonde Data. *J Geophys Res-Atmos*, **99**, 3655–3666.

Betts, A. K., 2004: Coupling between $CO_2$, water vapor, temperature, and radon and their

797 fluxes in an idealized equilibrium boundary layer over land. *J Geo Res*, **109**(D18),
798 D18103–. doi:10.1029/2003JD004420

799 Boers, R., S. Melfi, and S. P. Palm, 1995: Fractal Nature of the Planetary Boundary-
800 Layer Depth in the Trade-Wind Cumulus Regime. *Geophys Res Lett*, **22**, 1705–1708.

801 Bony, S., and K. Emanuel, 2005: On the role of moist processes in tropical intraseasonal
802 variability: Cloud-radiation and moisture-convection feedbacks. *J Atmos Sci*, **62**,
803 2770–2789.

804 Brient, F., and S. Bony, 2012: Interpretation of the positive low-cloud feedback
805 predicted by a climate model under global warming. *Climate Dynamics*.
806 doi:10.1007/s00382-011-1279-7

807 Brown, A. and Coauthors, 2002: Large-eddy simulation of the diurnal cycle of shallow
808 cumulus convection overland. *Q J Roy Meteor Soc*, **128**, 1075–1093.

809 Businger, J., J. Wyngaard, Y. Izumi, and E. Bradley, 1971: Flux-Profile Relationships in
810 the Atmospheric Surface Layer. *J Atmos Sci*., **28** (2), 181-189.

811 Chagnon, F. J. F., Bras, R. L., & Wang, J. 2004: Climatic shift in patterns of shallow
812 clouds over the Amazon. *Geo Res Letters*, **31** (24), L24212.
813 doi:10.1029/2004GL021188

814 Charney, J. G., 1975: Dynamics of Deserts and Drought in Sahel. *Q J Roy Meteor Soc*,
815 **101**, 193–202.

816 Charney, J. G., P. Stone, and W. J. Quirk, 1975: Drought in Sahara - Biogeophysical

817 Feedback Mechanism. *Science*, **187**, 434–435.

818 Crago, R., 1996: Conservation and variability of the evaporative fraction during the
819 daytime. *J Hydrol*, **180**, 173–194.

820 Crago, R., and W. Brutsaert, 1996: Daytime evaporation and the self-preservation of the
821 evaporative fraction and the Bowen ratio. *J Hydrol*, **178**, 241–255.

822 Cuesta, J., Edouart, D., Mimouni, M., & Flamant, P. H., 2008: Multiplatform
823 observations of the seasonal evolution of the Saharan atmospheric boundary layer in
824 Tamanrasset, Algeria, in the framework of the African Monsoon Multidisciplinary
825 Analysis field campaign conducted in 2006. *J Geo Res-Atmo* **113** (D00C07).
826 doi:10.1029/2007JD009417

827 D'Odorico, and I. Rodríguez-Iturbe, 2000: Space-time self-organization of mesoscale
828 rainfall and soil moisture. *Adv Water Resour*, **23**, 349–357.

829 Deardorff, J., 1979: Prediction of convective mixed-layer entrainment for realistic
830 capping inversion structure. *J Atmos Sci*, **36**, 424-436.

831 D'Andrea, F., Provenzale, A., Vautard, R., & De Noblet-, N. 2006: Hot and cool
832 summers: Multiple equilibria of the continental water cycle. *Geo Res Letters*, **33**
833 (L24807). doi:10.1029/2006GL027972

834 Del Genio, A. D., & Wu, J. 2010: The Role of Entrainment in the Diurnal Cycle of
835 Continental Convection. *J Climate*, **23** (10), 2722–2738.
836 doi:10.1175/2009JCLI3340.1

837 Delire, C., J. Foley, and S. Thompson, 2004: Long-term variability in a coupled
838 atmosphere-biosphere model. *J Climate*, **17**, 3947–3959.

839 Delworth, T., and S. Manabe, 1989: The Influence of Soil Wetness on Near-Surface
840 Atmospheric Variability. *J Climate*, **2**, 1447–1462.

841 Delworth, T., and S. Manabe, 1993: Climate Variability and Land-Surface Processes. *Adv*
842 *Water Resour*, **16**, 3–20.

843 Ek, M., and A. Holtslag, 2004: Influence of soil moisture on boundary layer cloud
844 development. *J Hydrometeorol*, **5**, 86–99.

845 Ek, M., and L. Mahrt, 1994: Daytime Evolution of Relative-Humidity at the Boundary-
846 Layer Top. *Mon Weather Rev*, **122**, 2709–2721.

847 Emanuel, K. A. (1994). *Atmospheric Convection*. Oxford University Press,.

848 Findell, K. L., P. Gentine, B. R. Lintner, and C. Kerr, 2011: Probability of afternoon
849 precipitation in eastern United States and Mexico enhanced by high evaporation. *Nat*
850 *Geosci*, **4**, 434–439, doi:10.1038/NGEO1174.

851 Gentine, P., D. Entekhabi, A. Chehbouni, G. Boulet, and B. Duchemin, 2007: Analysis of
852 evaporative fraction diurnal behaviour. *Agr Forest Meteorol*, **143**, 13–29,
853 doi:10.1016/j.agrformet.2006.11.002.

854 Gentine, P., D. Entekhabi, and J. Polcher, 2010: Spectral Behaviour of a Coupled Land-
855 Surface and Boundary-Layer System. *Bound-Lay Meteorol*, **134**, 157–180,
856 doi:10.1007/s10546-009-9433-z.

857 Gentine, P., D. Entekhabi, and J. Polcher, 2011a: The Diurnal Behavior of Evaporative
858 Fraction in the Soil-Vegetation-Atmospheric Boundary Layer Continuum. *J*
859 *Hydrometeorol*, **12**, 1530–1546, doi:10.1175/2011JHM1261.1.

860 Gentine, P., J. Polcher, and D. Entekhabi, 2011b: Harmonic propagation of variability in
861 surface energy balance within a coupled soil-vegetation-atmosphere system. *Water*
862 *Resour Res*, **47**, –, doi:10.1029/2010WR009268.

863 Gentine, P., A. Betts, K. Findell, B. Lintner, A. Tzella, and F. D'Andrea, 2012a: A
864 probabilistic-bulk model of coupled boundary layer and convection: 1) Clear-sky
865 case. *J. Atmos. Sci.* (submitted).
866 Gentine, P., A. Betts, K. Findell, B. Lintner, and F. D'Andrea, 2012b: A probabilistic-
867 bulk model of coupled boundary layer and convection: 2) Shallow convection
868 case. *J. Atmos. Sci.* (submitted).
869

870 Hohenegger, C., & Bretherton, C. S., 2011: Simulating deep convection with a shallow
871 convection scheme. *Atmos. Chem. Phys*, **11** (20), 10389–10406. doi:10.5194/acp-11-
872 10389-2011

873 Huang, H.-Y., & S. A. Margulis, 2011: Investigating the Impact of Soil Moisture and
874 Atmospheric Stability on Cloud Development and Distribution Using a Coupled
875 Large-Eddy Simulation and Land Surface Model. *J Hydrometeoro*, **12** (5), 787–804.
876 doi:10.1175/2011JHM1315.1

877 Isham, V., D. R. Cox, I. Rodríguez-Iturbe, A. Porporato, and S. Manfreda, 2005:

878 Representation of space-time variability of soil moisture. *P R Soc A*, **461**, 4035–4055,
879 doi:10.1098/rspa.2005.1568.

880 Katul, G. and Coauthors, 1999: Spatial variability of turbulent fluxes in the roughness
881 sublayer of an even-aged pine forest. *Bound-Lay Meteorol*, **93**, 1–28.

882 Katul, G. G., A. Porporato, E. Daly, A. C. Oishi, H.-S. Kim, P. C. Stoy, J.-Y. Juang, and
883 M. B. Siqueira, 2007: On the spectrum of soil moisture from hourly to interannual
884 scales. *Water Resour Res*, **43**, doi:10.1029/2006WR005356.

885 Katul, G., and M. Parlange, 1995: The spatial structure of turbulence at production
886 wavenumbers using orthonormal wavelets. *Bound-Lay Meteorol*, **75**, 81-108.

887 Katul, G., J. Albertson, C. Chu, and M. Parlange, 1994a: Intermittency in Atmospheric
888 Surface Layer Turbulence: The Orthonormal Wavelet Representation. *Wavelets in*
889 *Geophysics. Edited by Efi Foufoula-Georgiou*, **1**, 81.

890 Katul, G., M. Parlange, and C. Chu, 1994b: Intermittency, local isotropy, and non-
891 Gaussian statistics in atmospheric surface layer turbulence. *Physics of Fluids*.

892 Koster, R., and M. Suarez, 1994: The Components of a Svat Scheme and Their Effects on
893 a Gcms Hydrological Cycle, *Advances in Water Resources*, **17**, 61–78.

894 Laio, F., A. Porporato, C. Fernandez-Illescas, and I. Rodríguez-Iturbe, 2001: Plants in
895 water-controlled ecosystems: active role in hydrologic processes and response to
896 water stress - IV. Discussion of real cases. *Adv Water Resour*, **24**, 745–762.

897 Lhomme, J., and E. Elguero, 1999: Examination of evaporative fraction diurnal

898 behaviour using a soil-vegetation model coupled with a mixed-layer model. *Hydrol*
899 *Earth Syst Sc*, **3**, 259–270.

900 Li, B., and R. Avissar, 1994: The Impact of Spatial Variability of Land-Surface
901 Characteristics on Land-Surface Heat Fluxes. *J Climate*, **7**, 527-537.

902 Lilly, D., 1968: Models of Cloud-Topped Mixed Layers Under a Strong Inversion. *Q J*
903 *Roy Meteor Soc*, **94**, 292–309.

904 Lintner, B. R., Gentine, P., Findell, K. L., D'Andrea, F., Sobel, A. H., & Salvucci, G. D.
905 2012: An idealized prototype for large-scale land-atmosphere coupling. *J Climate, in*
906 *press*.

907 Mahrt, L., 1991: Boundary-Layer Moisture Regimes. *Q J Roy Meteor Soc*, **117**, 151–176.

908 Manfreda, S., M. McCabe, M. Fiorentino, and I. Rodríguez-Iturbe, 2007: Scaling
909 characteristics of spatial patterns of soil moisture from distributed modelling. *Adv*
910 *Water Resour*, **30** (10), 2145-2150.

911 Milly, P., and K. Dunne, 1994: Sensitivity of the Global Water Cycle to the Water-
912 Holding Capacity of Land. *J Climate*, **7**, 506–526.

913 Notaro, M., 2008: Response of the mean global vegetation distribution to interannual
914 climate variability. *Clim Dynam*, **30**, 845–854, doi:10.1007/s00382-007-0329-7.

915 Paradisi, P., R. Cesari, A. Donateo, D. Contini, and P. Allegrini, 2012: Scaling laws of
916 diffusion and time intermittency generated by coherent structures in atmospheric
917 turbulence. *Nonlinear Proc Geoph*, **19**, 113–126, doi:10.5194/npg-19-113-2012.

Petenko, I., and V. Bezverkhnii, 1999: Temporal scales of convective coherent structures derived from sodar data. Vol. 71 of, Meteorology and Atmospheric Physics, 105–116.

Pino, D., J. V.-G. de Arellano, and S.-W. Kim, 2006: Representing sheared convective boundary layer by zeroth- and first-order-jump mixed-layer models: Large-eddy simulation verification. *Journal of Applied Meteorology and Climatology*, **45**, 1224–1243.

Plaza, A. G., and J. A. Rogel, 2000: Spatial patterns and temporal stability of soil moisture across a range of scales in a semi- arid environment. *Hydrological Proc,* **14**, 1261-1277.

Porporato, A., 2009: Atmospheric Boundary-Layer Dynamics with Constant Bowen Ratio. *Bound-Lay Meteorol*, **132**, 227–240, doi:10.1007/s10546-009-9400-8.

Porporato, A., E. Daly, and I. Rodríguez-Iturbe, 2004: Soil water balance and ecosystem response to climate change. *Am Nat*, **164**, 625–632.

Rabin, R. M., S. Stadler, P. J. Wetzel, D. J. Stensrud, and M. Gregory, 1990: Observed Effects of Landscape Variability on Convective Clouds. *B Am Meteorol Soc*, **71**, 272–280.

Raupach, M., and J. Finnigan, 1995: Scale issues in boundary-layer meteorology: surface energy balances in heterogeneous terrain. *Hydrol Process*, **9**, 589-612.

Rigby, J. R., and A. Porporato, 2006: Simplified stochastic soil-moisture models: a look

938 at infiltration. *Hydrol Earth Syst Sc*, **10**, 861–871.

939 Rio, C., F. Hourdin, J. Y. Grandpeix, and J. P. Lafore, 2009: Shifting the diurnal cycle of
940 parameterized deep convection over land. *Geophys Res Lett*, **36**, –,
941 doi:10.1029/2008GL036779.

942 Robock, A., K. Vinnikov, C. Schlosser, N. A. Sperankaya, and Y. Xue, 1995: Use of
943 Midlatitude Soil-Moisture and Meteorological Observations to Validate Soil-
944 Moisture Simulations with Biosphere and Bucket Models. *J Climate*, **8**, 15–35.

945 Rodríguez-Iturbe, I., 2000: Ecohydrology: A hydrologic perspective of climate-soil-
946 vegetation dynamics. *Water Resour Res*, **36**, 3–9.

947 Rodríguez-Iturbe, I., G. Vogel, R. Rigon, D. Entekhabi, F. Castelli, and A. Rinaldo, 1995:
948 On the Spatial-Organization of Soil-Moisture Fields. *Geophys Res Lett*, **22**, 2757–
949 2760.

950 Rodríguez-Iturbe, I., P. D'Odorico, A. Porporato, and L. Ridolfi, 1999: On the spatial and
951 temporal links between vegetation, climate, and soil moisture. *Water Resour Res*, **35**,
952 3709–3722.

953 Ronda, R., B. van den Hurk, and A. A. M. Holtslag, 2002: Spatial heterogeneity of the
954 soil moisture content and its impact on surface flux densities. *J Hydrometeorol*, **3**, (5)
955 556-570.

956 Skoien, J., G. Bloschl, and A. Western, 2003: Characteristic space scales and timescales
957 in hydrology. *Water Resour Res*, **39**, –, doi:10.1029/2002WR001736.

958 Sorbjan, Z., 2008: Local scales of turbulence in the stable boundary layer. *Bound-Lay*
959 *Meteorol,* **127**, 261–271, doi:10.1007/s10546-007-9260-z.

960 Stéfanon, M., Drobinski, P., D'Andrea, F., Lebeaupin-Brossier, C., Bastin, S., 2012: Soil
961 moisture-temperature feedbacks at meso-scale during summer heat waves over
962 Western Europe, *Clim Dyn*, submitted

963 Taylor, C. M., Gounou, A., Guichard, F., Harris, P. P., Ellis, R. J., Couvreux, F., & De
964 Kauwe, M., 2011: Frequency of Sahelian storm initiation enhanced over mesoscale
965 soil-moisture patterns. *Nature Geoscience*, **4** (7), 430–433. doi:10.1038/ngeo1173

966 Taylor, C. M., R. A. M. de Jeu, F. Guichard, P. P. Harris, and W. A. Dorigo, 2012:
967 Afternoon rain more likely over drier soils. *Nature*, doi:10.1038/nature11377.

968 van Heerwaarden, C. C., and J. V.-G. de Arellano (2008), Relative humidity as an
969 indicator for cloud formation over heterogeneous land surfaces, *J Atmos Sci*, ***65***(10),
970 3263–3277, doi:10.1175/2008JAS2591.1.

971 van Heerwaarden, C. C., J. V.-G. de Arellano, A. F. Moene, and A. A. M. Holtslag
972 (2009), Interactions between dry-air entrainment, surface evaporation and convective
973 boundary-layer development, *Q J Roy Meteor Soc*, ***135***(642), 1277–1291,
974 doi:10.1002/qj.431.

975 Wang, J., Bras, R. L., & Eltahir, E. 2000, The impact of observed deforestation on the
976 mesoscale distribution of rainfall and clouds in Amazonia. *J Hydrometeor*, *1*(3), 267–
977 286.

978 Western, A., R. Grayson, and G. Bloschl, 2002: Scaling of soil moisture: A hydrologic

perspective. *Annu Rev Earth Pl Sc*, **30**, 149–180.

Western, A., S. Zhou, R. Grayson, T. McMahon, G. Bloschl, and D. Wilson, 2004: Spatial correlation of soil moisture in small catchments and its relationship to dominant spatial hydrological processes. *J Hydrol*, **286**, 113–134, doi:10.1016/j.jhydrol.2003.09.014.

Westra, D., Steeneveld, G. J., & Holtslag, A. A. M. (2012). Some Observational Evidence for Dry Soils Supporting Enhanced High Relative Humidity at the Convective Boundary Layer Top. *J Hydromet*, 1347–1358.

Wheater, H. and Coauthors, 2000: Spatial-temporal rainfall fields: modelling and statistical aspects. *Hydrol Earth Syst Sc*, **4**, 581–601.

Wu, C.-M., B. Stevens, and A. Arakawa, 2009: What Controls the Transition from Shallow to Deep Convection? *J Atmos Sci*, **66**, 1793–1806, doi:10.1175/2008JAS2945.1.

Wulfmeyer, V., 1999: Investigation of turbulent processes in the lower troposphere with water vapor DIAL and radar-RASS. *J Atmos Sci*, **56**, 1055–1076.

Wyant, M. C., Bretherton, C. S., Blossey, P. N., & Khairoutdinov, M., 2012: Fast cloud adjustment to increasing CO 2in a superparameterized climate model. *J. Adv. Model. Earth Syst*, *4*, M05001. doi:10.1029/2011MS000092

Xue, Y., and J. Shukla, 1993: The Influence of Land-Surface Properties on Sahel Climate .1. Desertification. *J Climate*, **6**, 2232–2245.

# Tables

**Table 1. List of variables and parameters.**

| ***Symbol*** | ***Description*** |
|---|---|
| $A_0$ | Maximum diurnal available energy at the surface |
| $B_0$ | Surface Bowen ratio |
| $B_{inv}$ | Inversion Bowen ratio |
| $C_p$ | Specific heat of dry air |
| $EF$ | Evaporative fraction |
| $g$ | Gravity acceleration |
| $G$ | Soil heat flux |
| $h$ | Boundary-layer height |
| $H$ | Sensible heat flux at the surface |
| $L_v$ | Latent heat of vaporization of water |
| $p_0$ | Reference pressure of the potential temperature computation (1000mb) |
| $p$ | Pressure at the top of the mixed layer |
| $q$ | Specific humidity |
| $\overline{q}$ | Mixed-layer specific humidity |

| | |
|---|---|
| $q_{f0}$ | Free-troposphere value of specific humidity at the surface |
| $q_s$ | Saturated specific humidity (at boundary layer top) |
| $R_d$ | Gas constant of dry air |
| $R_n$ | Net radiation at the surface |
| $R_v$ | Gas constant of water vapor |
| $RH$ | Relative humidity |
| $t$ | Time |
| $t_0$ | Sunset |
| $T$ | Temperature of the air |
| $\alpha$ | Entrainment efficiency (~0.2) |
| $\Delta q$ | Jump in specific humidity at the boundary layer top |
| $\Delta\theta$ | Jump in potential temperature at the boundary layer top |
| $\gamma_q$ | Free-tropospheric lapse rate of specific humidity |
| $\gamma_\theta$ | Free-tropospheric lapse rate of potential temperature $\theta$ |
| $\rho$ | Density of dry air |
| $\theta$ | Potential temperature |
| $\overline{\theta}$ | Mixed-layer potential temperature |

| | |
|---|---|
| $\theta_{f0}$ | Free-troposphere value of potential temperature at the surface |
| $\Gamma_{dry}$ | Dry adiabatic temperature lapse rate |
| $\Gamma_{moist}$ | Moist adiabatic temperature lapse rate |
| $\lambda E$ | Latent heat flux at the surface |

# List of Figures

FIG. 4: Cloud base (LCL) at the time of cloud occurrence as a function of evaporative fraction for a maximum available energy $A_0$ = 500 W m$^{-2}$ and for varying values of free-tropospheric humidity and free-tropospheric surface potential temperature. The free troposphere is more humid to the right and warmer to the bottom. Color dots refer to the AMMA profiles. Similar colors are used as in FIG. 1. Black dot is Cabauw data.

FIG. 5: Root of the sensitivity of the relative humidity at the mixed layer top $\frac{dRH(h)}{dEF}$ at solar noon for a maximum diurnal available energy $A_0$ = 500Wm$^{-2}$. The curve delineates the region of positive and negative sensitivity of the relative humidity tendency to EF. In the positive region above the curve (denoted by a + sign), a rise in EF increases the relative humidity at the mixed-layer top and therefore the likelihood of clouds. An opposite behavior is observed in the negative region (denoted by a - sign). Color dots refer to the AMMA profiles. Similar colors are used as in FIG. 1. Black dot is Cabauw data.

FIG. 6: Ratio of Factor1 (direct moistening) to Factor2 (entrainment effect) in $\log_{10}$ scale, as a function of evaporative fraction (EF) and inversion Bowen ratio $B_{inv}$. Values above 0 represent an advantage of the direct moistening over the free-tropospheric entrainment and drying. Color dots refer to the AMMA profiles. Similar colors are used as in FIG. 1. Black dot is Cabauw data.

FIG. 7: Ratio of first term of the thermodynamic factor (departure between dry and moist adiabatic) to the second term (dilatation effect) in $\log_{10}$ scale, as a function of evaporative

fraction (EF) and free-tropospheric stability. The results are relatively insensitive to the moistening of the free troposphere and reference temperature. The crossover region between the preponderance of each factor is plotted in bold black line. Color dots refer to the AMMA profiles. Similar colors are used as in FIG. 1. Black dot is Cabauw data.

FIG. 8: Ratio of the dynamic to thermodynamic factors of the relative humidity tendency. Gray line depicts the limit between dry vs. wet soil advantage regimes. Bold black line depicts crossover between positive and negative values. Color dots refer to the AMMA profiles. Similar colors are used as in FIG. 1. Black dot is Cabauw data.

FIG. 9: Difference between the equivalent potential temperature of the mixed layer and the saturation equivalent potential temperature of the free troposphere just above the inversion ($h_+$) at sunset. Negative (blue) regions denote stratocumulus occurrence and positive (warm colors) depict the occurrence of shallow or deep convection. White areas denote regions without clouds. Black bold contour depicts the crossover between positive and negative regions.

# Figures

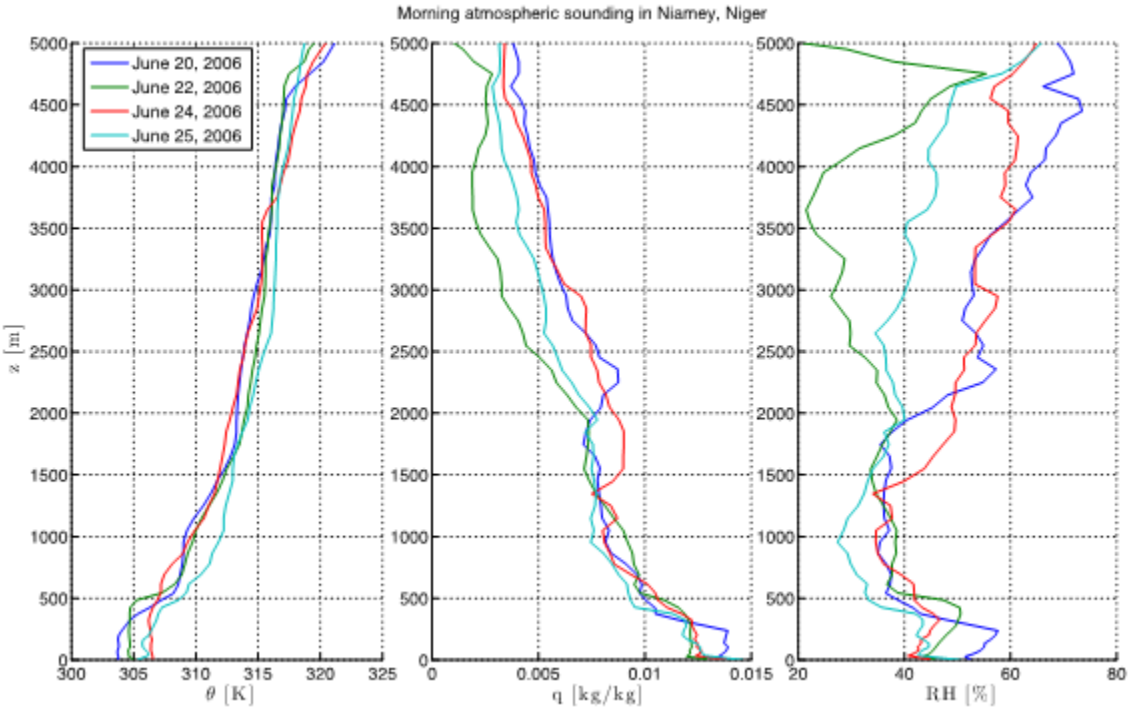


FIG. 1: Early morning soundings of (left) potential temperature, (middle) specific humidity and (right) relative humidity over Niamey, Niger during the African Monsoon Multidisciplinary Analysis (AMMA) field campaign.

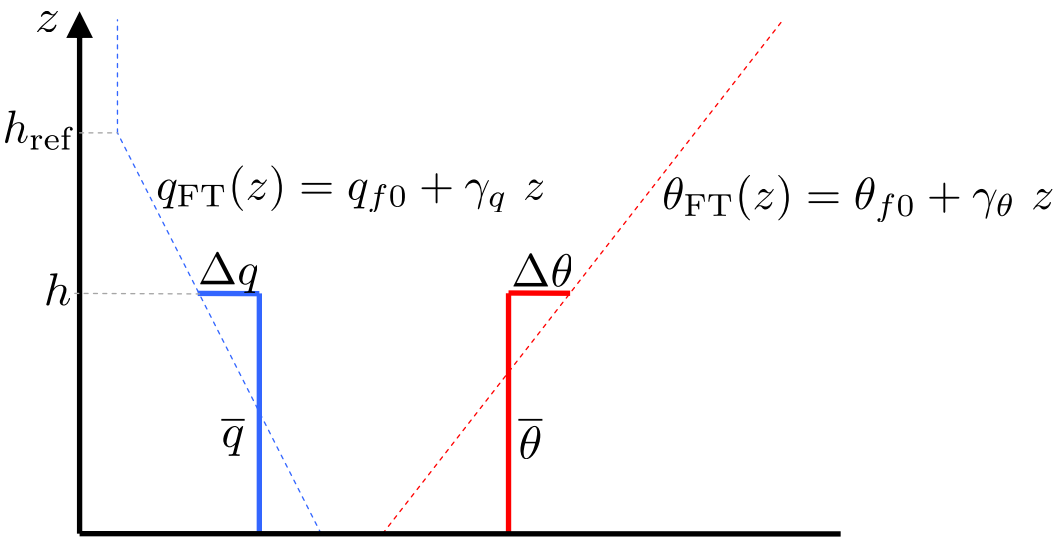


1071

1072 FIG. 2: Mixed-layer model of the boundary layer. The inversion Bowen ratio is

1073 $B_{\mathrm{inv}} = C_p \gamma_\theta / L_v \gamma_q$.

1074
1075

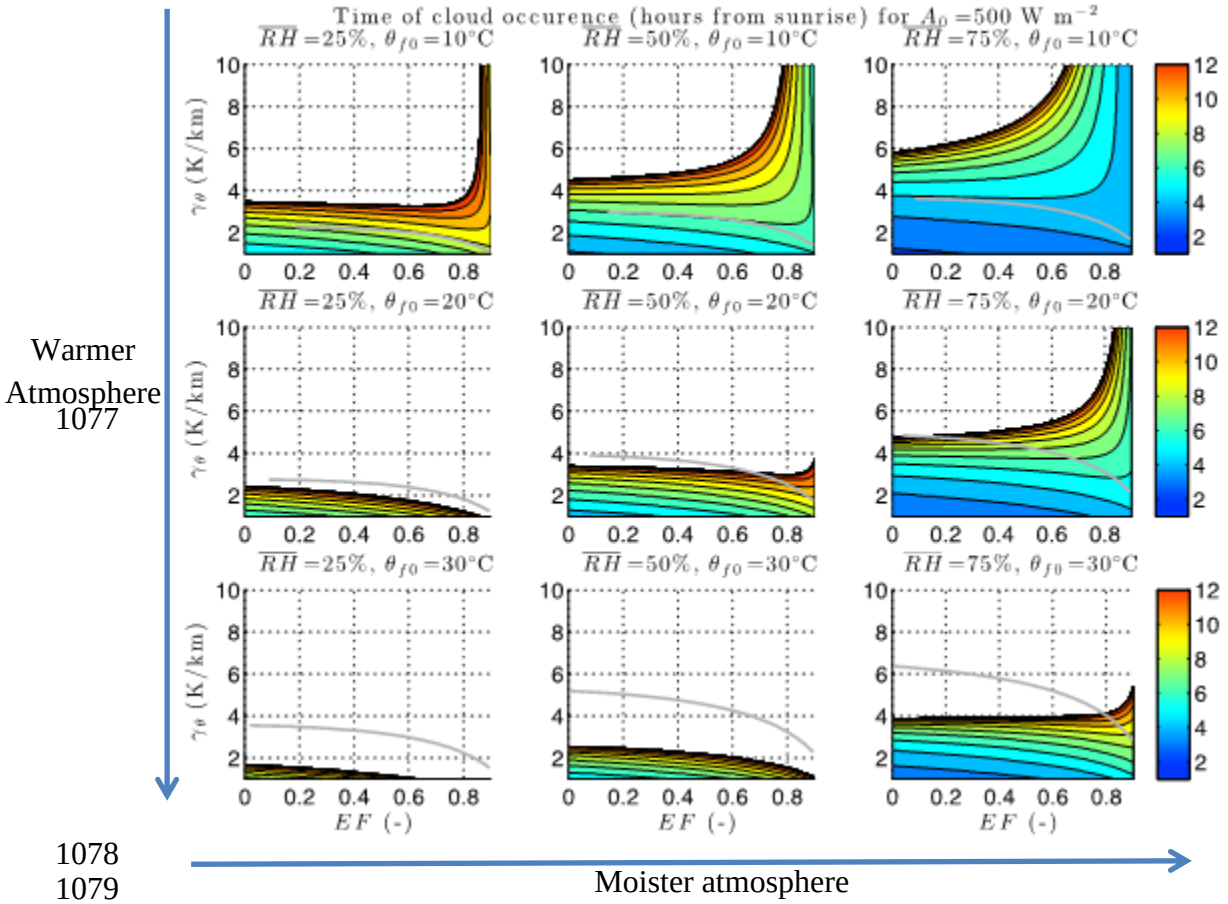


FIG. 3: Time of cloud occurrence from sunrise as a function of evaporative fraction for a maximum available energy $A_0$ = 500 W m-2 and for varying values of free-tropospheric humidity and free-tropospheric surface potential temperature. The free troposphere is more humid to the right and warmer to the bottom. Gray bold line delimitate the positive sensitivity of the relative humidity region (top) “moist soil advantage” from the negative region “dry soil advantage”.

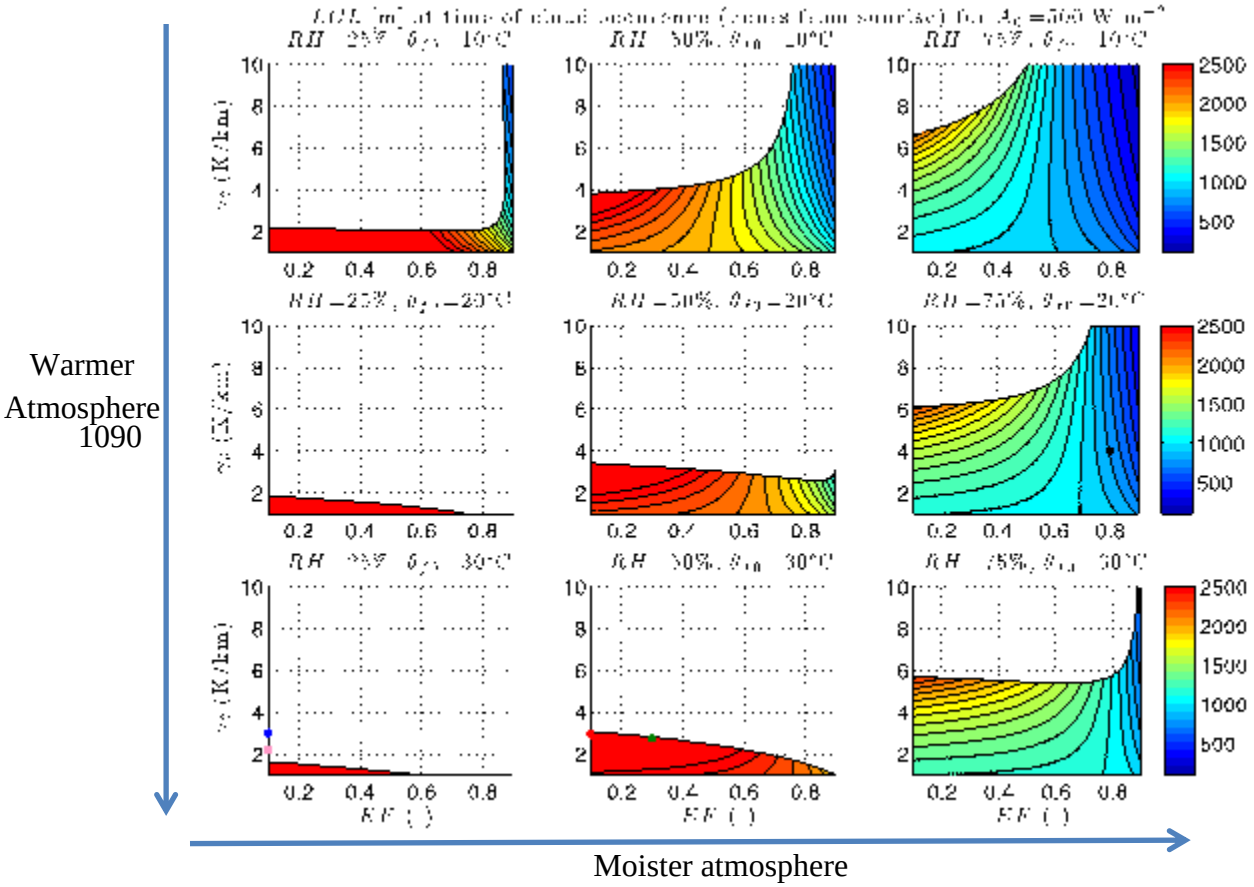


FIG. 4: Cloud base (LCL) at the time of cloud occurrence as a function of evaporative fraction for a maximum available energy $A_0$ = 500 W m$^{-2}$ and for varying values of free-tropospheric humidity and free-tropospheric surface potential temperature. The free troposphere is more humid to the right and warmer to the bottom. Color dots refer to the AMMA profiles. Similar colors are used as in FIG. 1. Black dot is Cabauw data.

1103

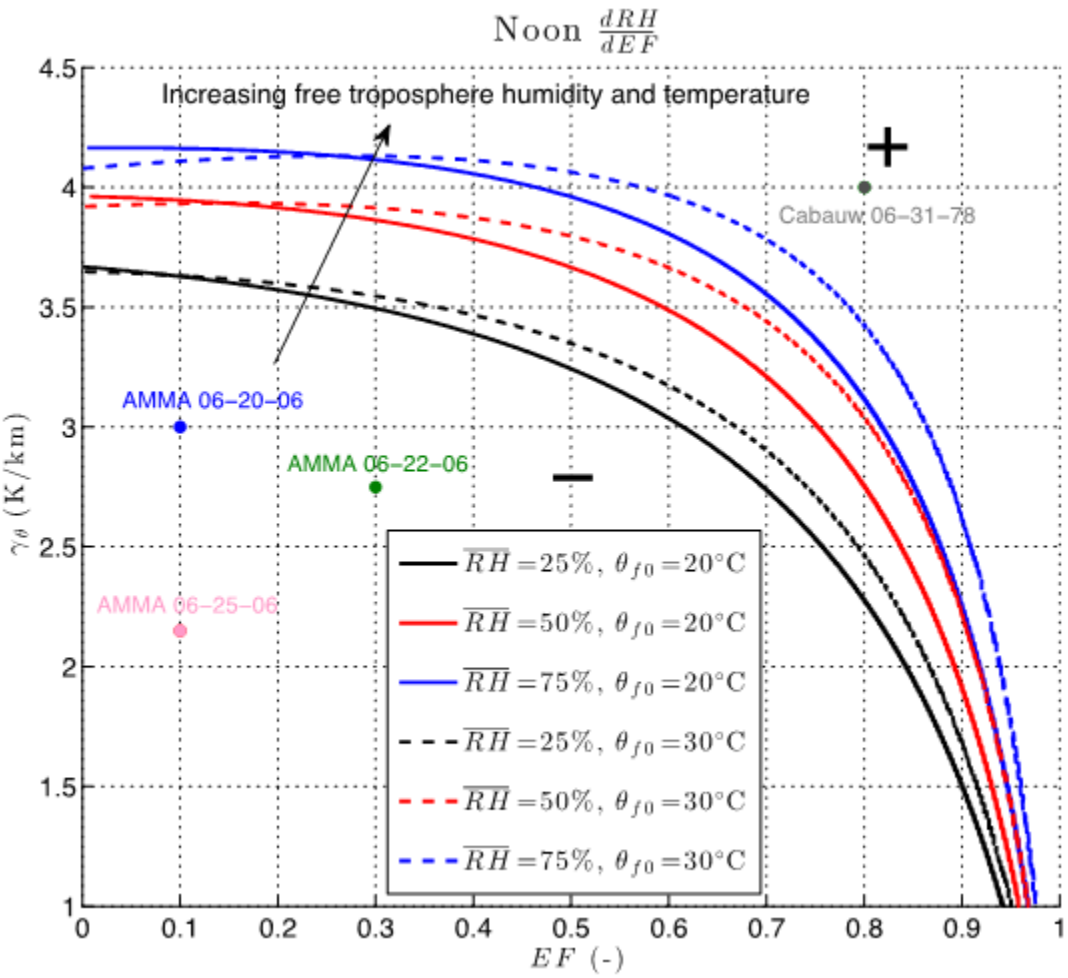


1104 FIG. 5: Root of the sensitivity of the relative humidity at the mixed layer top $\frac{dRH(h)}{dEF}$ at

1105 solar noon for a maximum diurnal available energy $A_0$ = 500Wm$^{-2}$. The curve delineates

1106 the region of positive and negative sensitivity of the relative humidity tendency to EF. In

1107 the positive region above the curve (denoted by a + sign), a rise in EF increases the

1108 relative humidity at the mixed-layer top and therefore the likelihood of clouds. An

1109 opposite behavior is observed in the negative region (denoted by a - sign). Color dots

1110 refer to the AMMA profiles. Similar colors are used as in FIG. 1. Black dot is Cabauw

1111 data.

1112

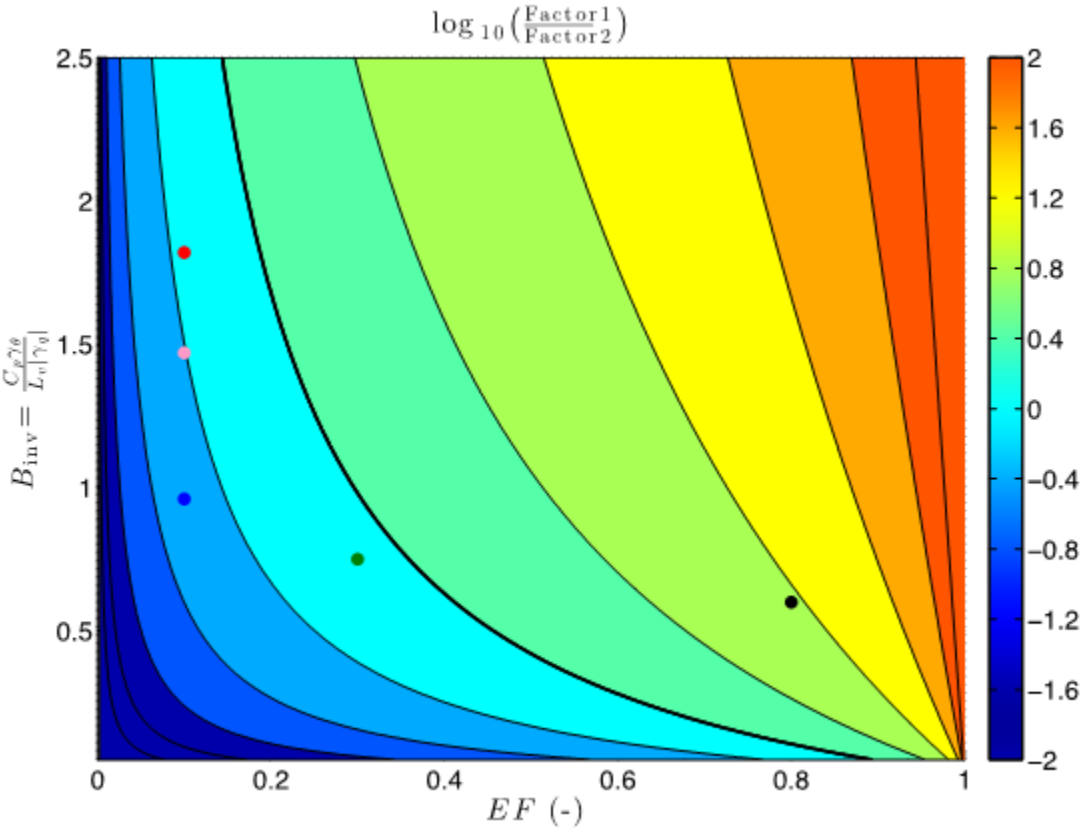


FIG. 6: Ratio of Factor1 (direct moistening) to Factor2 (entrainment effect) in $\log_{10}$ scale, as a function of evaporative fraction (EF) and inversion Bowen ratio $B_{inv}$. Values above 0 represent an advantage of the direct moistening over the free-tropospheric entrainment and drying. Color dots refer to the AMMA profiles. Similar colors are used as in FIG. 1. Black dot is Cabauw data.

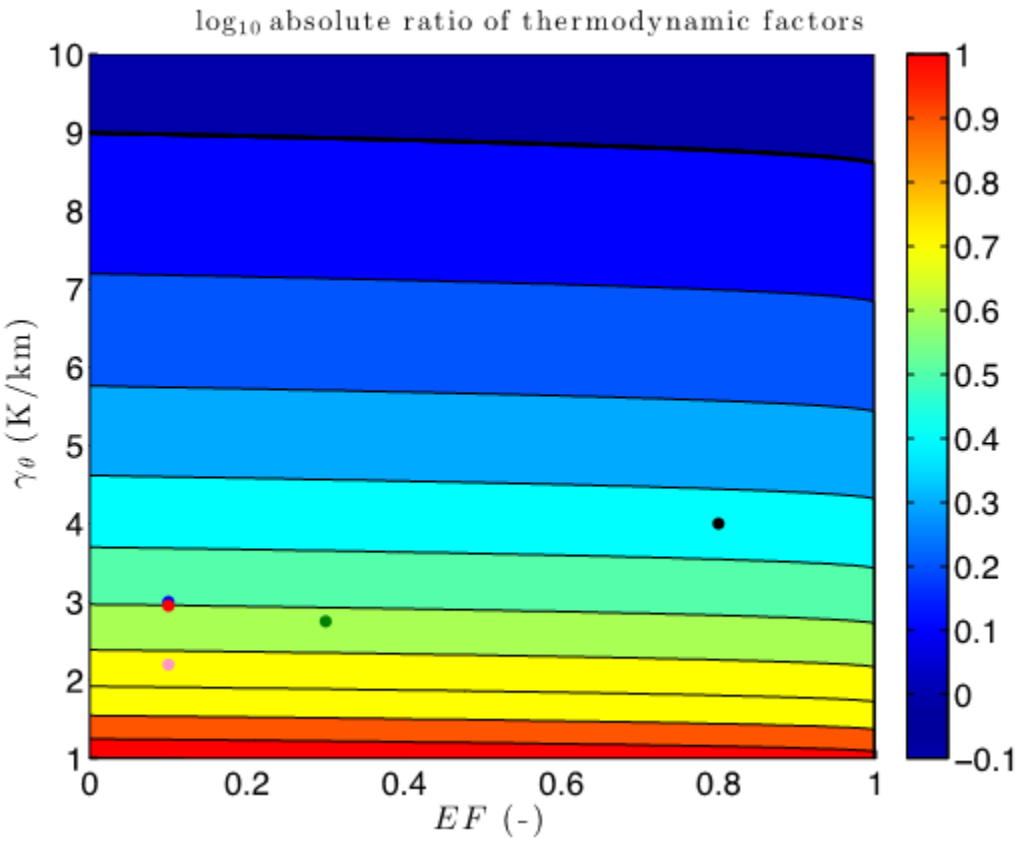


FIG. 7: Ratio of first term of the thermodynamic factor (departure between dry and moist adiabatic) to the second term (dilatation effect) in $\log_{10}$ scale, as a function of evaporative fraction (EF) and free-tropospheric stability. The results are relatively insensitive to the moistening of the free troposphere and reference temperature. The crossover region between the preponderance of each factor is plotted in bold black line. Color dots refer to the AMMA profiles. Similar colors are used as in FIG. 1. Black dot is Cabauw data.

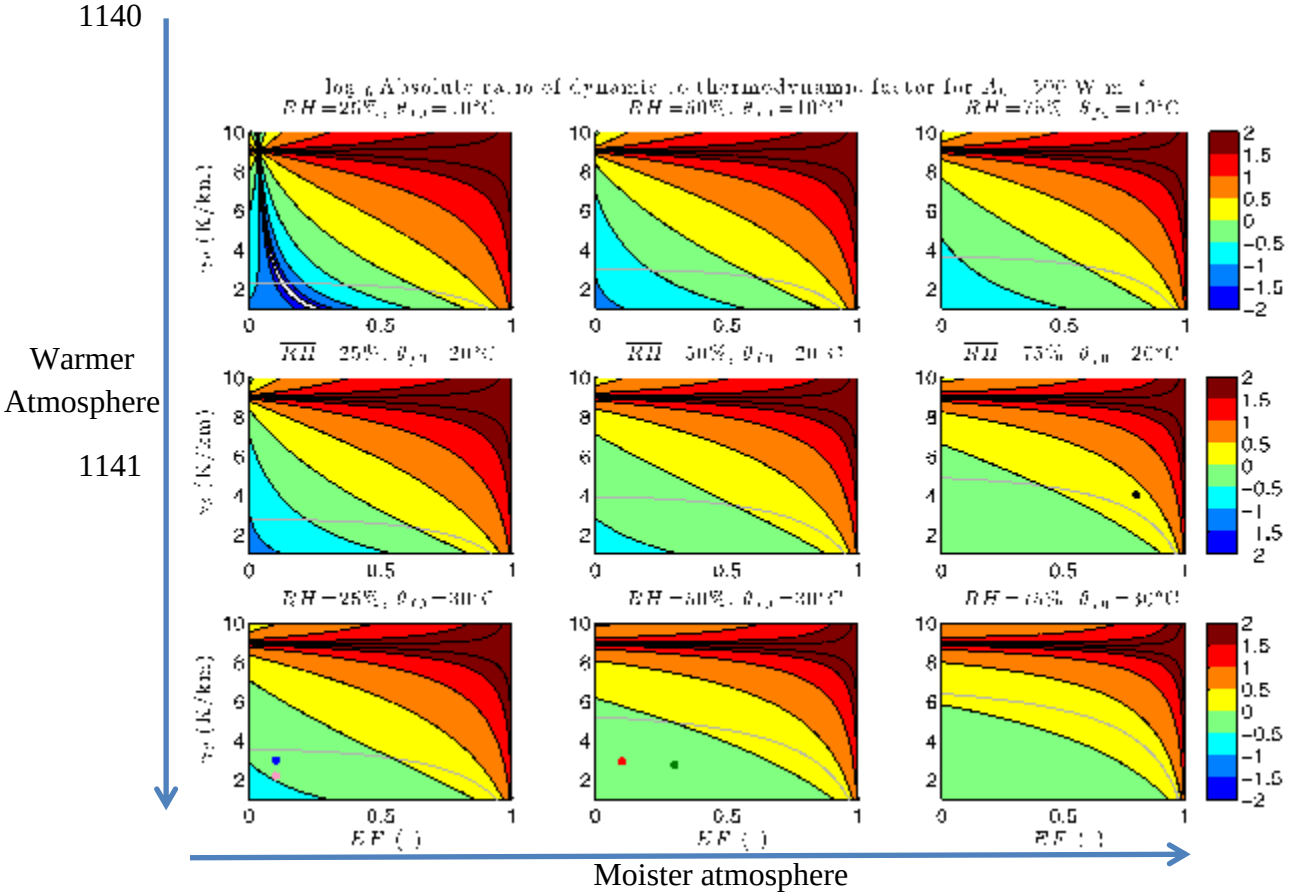


FIG. 8: Ratio of the dynamic to thermodynamic factors of the relative humidity tendency. Gray line depicts the limit between dry vs. wet soil advantage regimes. Bold black line depicts crossover between positive and negative values. Color dots refer to the AMMA profiles. Similar colors are used as in FIG. 1. Black dot is Cabauw data.

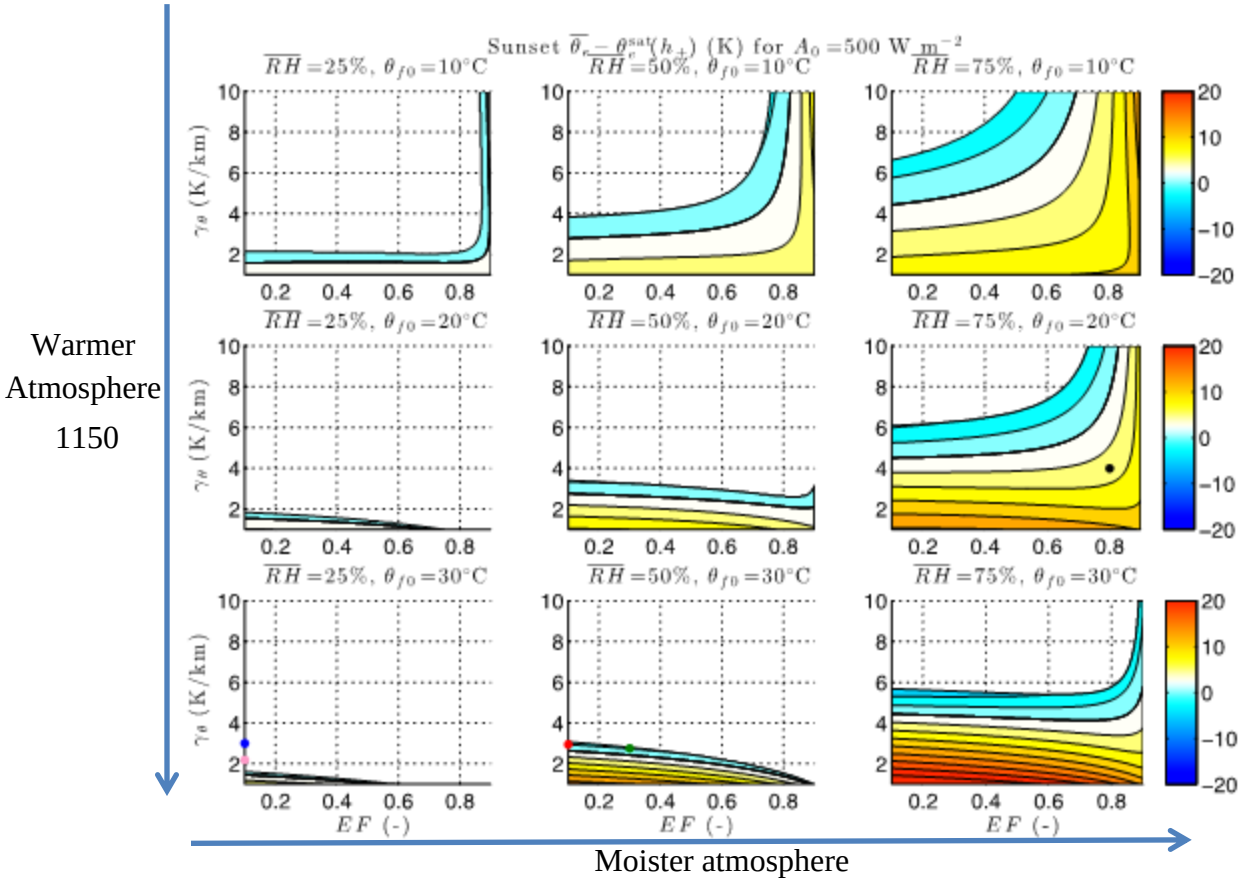


FIG. 9: Difference between the equivalent potential temperature of the mixed layer and the saturation equivalent potential temperature of the free troposphere just above the inversion ($h_+$) at sunset. Negative (blue) regions denote stratocumulus occurrence and positive (warm colors) depict the occurrence of shallow or deep convection. White areas denote regions without clouds. Black bold contour depicts the crossover between positive and negative regions.